Hindawi Publishing Corporation
Advances in Tribology
Volume 2015, Article ID 815179, 31 pages
http://dx.doi.org/10.1155/2015/815179

Research Article

Experimental Evaluation of Erosion of Gunmetal under Asymmetrical Shaped Sand Particle

Mohammad Asaduzzaman Chowdhury,[1] Uttam Kumar Debnath,[1] Dewan Muhammad Nuruzzaman,[2] and Md. Monirul Islam[3]

[1]*Department of Mechanical Engineering, Dhaka University of Engineering and Technology, Gazipur, Gazipur 1700, Bangladesh*
[2]*Faculty of Manufacturing Engineering, Universiti Malaysia Pahang, 26600 Pekan, Pahang Darul Makmur, Malaysia*
[3]*Bangladesh Chemical Industries Corporation, Dhaka 1000, Bangladesh*

Correspondence should be addressed to Mohammad Asaduzzaman Chowdhury; asadzmn2014@yahoo.com

Received 19 May 2015; Revised 11 July 2015; Accepted 26 July 2015

Academic Editor: Navin Chand

The erosion characteristics of gunmetal have been evaluated practically at different operating conditions. Asymmetrical silica sand (SiO_2) is taken into account as erodent within range of 300–600 μm. The impact velocity within 30–50 m/sec, impact angle 15–900, and stand off distance 15–25 mm are inspected as other relevant operating test conditions. The maximum level of erosion is obtained at impact angle 15° which indicates the ductile manner of the tested gunmetal. The higher the impact velocity, the higher the erosion rate as almost linear fashion is observed. Mass loss of gunmetal reduces with the increase of stand-off distance. A dimensional analysis, erosion efficiency (η), and relationship between friction and erosion indicate the prominent correlation. The test results are designated using Taguchi's and ANOVA concept. S/N ratio indicates that there are 1.72% deviations that are estimated between predicted and experimental results. To elaborately analyze the results, ANN and GMDH methods are mentioned. After erosion process of tested composite, the damage propagation on surfaces is examined using SEM for the confirmation of possible nature of wear behavior. The elemental composition of eroded test samples at varying percentage of gunmetal is analyzed by EDX analysis.

1. Introduction

Erosion is described as the progressive loss of original material from a solid surface due to mechanical interaction between the surfaces and impinge solid or liquid particle which may be a multicomponent fluid or impinging solid or liquid particles also. Erosive damages of different materials in modern technological systems are very concerning issue for sustainability of the materials with these adverse conditions. In advanced engineering and industrial field, light weight of materials has several applications for minimizing the operating as well as initial investment cost. In different environmental conditions, wind turbine, blower fan blade, hydraulic turbine impellers, and the moving components of ship, aircraft, train, and automobile structure made by different metals and alloys experience the difficulty of impingement of solid particles in the form of erosion. Gunmetal can be used extensively in erosive wear environment for its simple manufacturing technique, suitability for design of different systems and mechanisms, and lower manufacturing cost. Concerning these facts, the gunmetal has been chosen as test samples to examine the erosion resistance at different operating conditions so that the exact nature of erosion can be identified.

The researches have been done by the different tribology research groups [1–6] who realized that erosive wear of materials is related to the various factors such as impingement angle, impact velocity, particle size, particle shape, particle type, particle flux, temperature, nozzle geometry, type of materials, hardness of the materials, stand-off distance, test duration, and roughness of the tested materials. Among these factors impingement angle and impact velocity have been

recognized as two parameters that noticeably influence the erosion rates of different materials [7]. The erosive behavior of AISI 440C stainless steel and a cermet has been conducted by researchers [8] who observed that both of the materials exhibited noticeable plasticity during impact conditions, but in case of stainless steels which has been characterized by being more ductile in nature. The blending conditions of materials, temperature, pressure, and flow can create the erosive-corrosive wear especially for metal and alloys [9]. Rather than different mechanical properties and operating conditions material hardness has certain amount of role to propagate erosion damage throughout the metals and alloys [10].

The previous works [1–10] on metal and alloys varying with different operating and processing conditions as well as mechanical properties and varying percentage of material-combinations on erosion of materials cannot suggest any unique trends of the results. Therefore, the objective of this work is to investigate the erosive wear performance of gunmetal under several test conditions to understand the possible nature of erosion. A dimensional analysis indicates that there is a significant relation between erosion rate and Uttam Number (U. No.). In addition to that, dependency level of theoretical friction coefficient and erosion rate are observed. To analyze the obtained results in board concept, Taguchi, ANOVA, erosion efficiency, ANN, and GMDH approach have been discussed. The morphology of damage surface incorporating possible nature has been analyzed using SEM. The elemental composition of different locations of eroding gunmetal surfaces is obtained by EDX analysis.

2. Experimental Details

2.1. Materials Properties, Preparation, and Method of Erosion Measurement. The measured mechanical properties of tested gunmetal are listed in Table 1. Rectangle type specimens with a size of 50 mm × 30 mm × 5 mm were prepared by utilizing a diamond cutter from injection moulded plaques. Before the erosive wear tests, all specimens were cleaned with acetone. Great care was given to ensure clean surface before and after wear tests. Sand and dust particles were cleaned after erosion test with air blasting and then balanced carefully.

Different grain size (300–355, 355–500, and 500–600 microns) with irregular shape (combination of rounded, slightly rounded, and angular) dry quartz type silica sand (hardness 42, 43.2, and 44 MPa, density 1436, 1440, and 1443 kg/m^3) of chemical composition SiO_2 was used as an erodent particle. Motor type vibration sieve machine (model: VSS-T, Vinsyst Technologies, ISO 900, India) with measuring range 97 μm to 4 mm was used to measure the particle size.

The weight of the samples before and after erosion process was measured by using precision digital electronic balance (model: SP404D, Sciencetech Inc., USA). Erosion rates were calculated from the differences of weight loss by considering unit of time ($E_R = (W_{\text{before}} - W_{\text{after}})/\text{Time}$).

The flow pattern of abrasive particle is related to different factors, such as type of erodent materials, chemical composition, hardness, density, particle shape, and particle size and impact resistance. At the time of the experiment, under lower impact velocity, the pattern of flow of abrasive particle was realized almost similar to the laminar nature but with the increase of velocity laminar as well as turbulent combination of flow pattern being observed. But the changing of impact angles may have some role for characterizing the flow of abrasive particle. In fact, there were different modes of effect of flowing abrasive under different operating conditions. In this context, elastic/plastic deformation by sliding-rubbing grain movement, elastic/plastic deformation by rolling grain movement, chip formation (microcutting) by rubbing grain movement, ridges formation by rubbing and rolling grain movement, and low-cycle fatigue wear were identified. To ensure the exact abrasive flow, more researches can be conducted in future study relevant to experimental and analytical point of view.

Table 1: Mechanical and related properties of gunmetal.

Property	Standard value (S.I.)	Actual or measured data	Units (S.I.)
Density	8719	8710	kg/m^3
Tensile yield strength	110	118	MPa
Ultimate tensile strength	220	225	MPa
Hardness	80	85	HB

2.2. Test Apparatus. A sand blast erosive wear testing device was designed and fabricated to understand the erosion process, as shown in Figure 1. In this sand blast erosion test rig, sand was ejected from the nozzle by high pressure air to strike the test sample. A geared motor was fixed to a horizontal frame and connected to a cylindrical hollow shaft by a belt and pulley. A hopper was connected to the upper portion of the cylindrical hollow shaft by threads.

An air-sand mixing chamber was connected to the other part of cylindrical hollow shaft, the upper part of which was connected with the compressor with a hose and the lower part attached to a 5 mm converging nozzle. Compressor pressure was controlled by a pressure valve attached to the upper part of the mixing chamber. The motor was run at 60 rpm to transmit sand from the hopper to the mixing chamber at a constant rate via the feed gear. Air and sand were mixed in the mixing chamber and, as a result of high air pressure, sand was ejected through the nozzle at high impingement velocity. A sample holder was fixed in the horizontal plane and was designed to maintain the stand-off distance and to vary the test sample angle from 0 to 90°.

2.3. Selection of Number of Observations. The criteria of selection of number of observations of each experiment are the justification of ensuring the accuracy level of tested results. The equation mentioned below is used to validate the

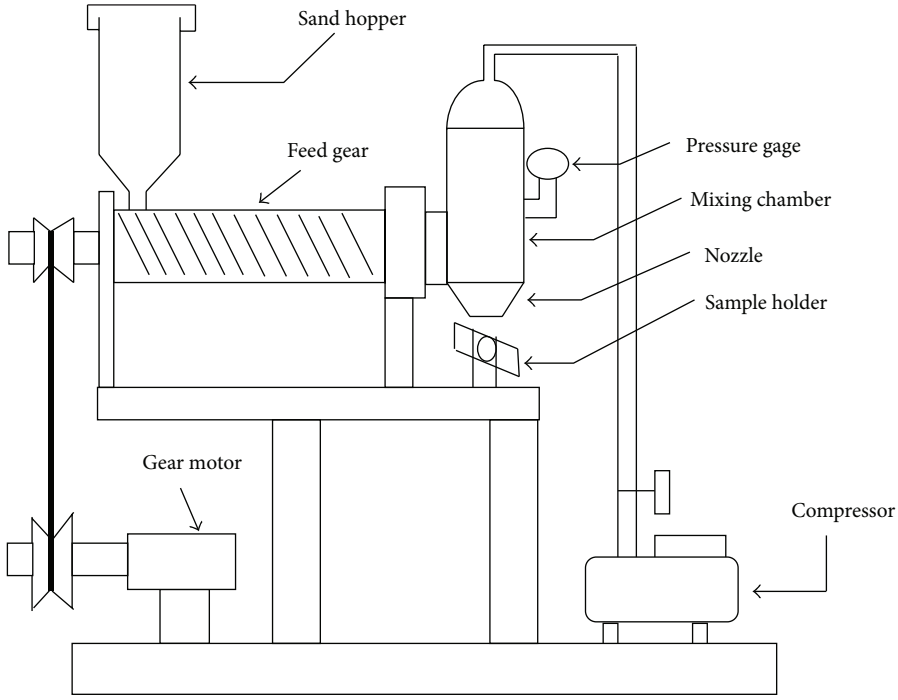

Figure 1: Schematic diagram of the solid particle erosion rig.

selection of number of cycles under certain confidence level within certain accuracy:

$$n = \left(\frac{zs}{A\overline{x}}\right)^2, \tag{1}$$

where n is number of observations that should be taken to provide desired accuracy. Z is Normal deviate for desired confidence level. $S = \sqrt{(\sum x^2 - (\sum x)^2/n')/(n'-1)}$ is estimated standard deviation for the distribution of element time based on observations already made. A is accuracy desired expressed as decimal fraction of true value. $\overline{x}$ is mean of the erosion values, already collected. n' is number of observations already made.

For the confirmation of accuracy of the test results, the selections of the number of experimental observations were selected using (1). The basis of number of repeatabilities of each experiment at identical test conditions ensures the confidence level within desired accuracy. At the time of designing the number of observations, 95% confidence level within 2% accuracy was considered.

2.4. Particles Velocity Measuring Method. The double disc process was adapted to estimate the impingement velocity of solid particles. The method used for calculating particle velocity is illustrated in Figure 2. A 15 mm diameter vertical circular stainless steel 304 rod was connected at the top and bottom with 150 mm diameter circular plates and a 1.5 mm hole in the top plate. The high velocity sand was directed on the static top plate hole and, as a consequence, color damage (A) was created on the static lower plate. Then the two horizontal plates were rotated, further color damage (B) was obtained on the lower plate by the sand. The angular displacements of A and B were estimated, and the following formula (2) used to estimate the impingement velocity:

$$V = \frac{2\pi RvL}{S}, \tag{2}$$

where L is the distance between the top and bottom plates, v is the rotational rpm of top and bottom plates, R is the radius from the center of the bottom plate to point B, and S is the angular distance between the two areas of color damage. The impingement velocity calibrations at different pressures are summarized in Table 2.

2.5. ANN Concept. In general, erosive wear is related to variable factors such as impingement velocity, impingement angle, particle size, and stand-off distance. In addition, solid particle flowing parameters are important conditions that affect erosion. Although the solid particle flowing technique has some unknown parameters, these factors should not be ignored, in spite of the difficulty in determining or identifying them. Numerical or finite element techniques can be used to identify hidden factors. However, these techniques tend to be complex, and simple linear regression method does not adequately explain the nonlinearity of the results. Therefore, artificial neural networks (ANN) can be utilized, and ANN models can predict outcomes with a certain level of accuracy, even when the variable relationships are uncertain. In ANN, data-based phenomena are used to predict and examine property-based parameters. Our ANN methodology expresses stored data development, implementation code, and prediction-based outcomes in erosive wear.

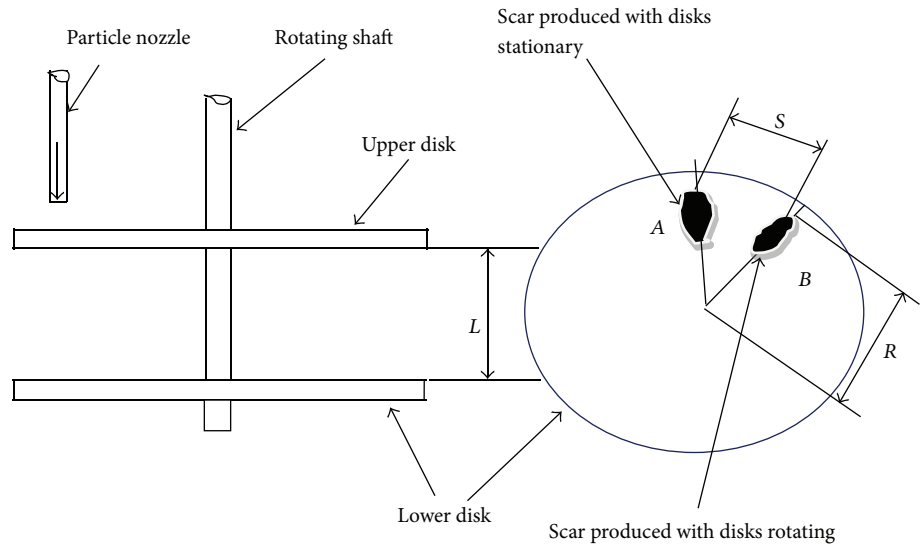

Figure 2: Schematic diagram of methodology used for velocity calibration.

Table 2: The impact velocity calibration at various pressure.

Pressure (bar)	Speed of the rotating disc (rpm)	Linear separation of two marks (mm)	Impact velocity (m/s)	Average impact velocity (m/s)
3.5	4700	6.2	49.61	50
		6.3	48.83	
		6.1	50.42	
3	4500	7.4	39.98	40
		7.2	40.88	
		7.4	39.78	
2	4000	8.7	30.07	30
		8.5	30.75	
		8.6	30.42	

Table 3: Selection of input criterion for training.

Input parameters for training	Values
Error tolerance	0.0002
Learning parameter (β)	0.2
Momentum parameter (α)	0.003
Noise factor (NF)	0.0001
Maximum cycles for simulations	2000000
Slope parameter (£)	0.07
Number of hidden layer neurons	12
Number of input layer neurons (I)	4
Number of output layer neurons (O)	1

2.6. NEURAL Analysis. In this analysis, impact velocity, impact angle, erodent size, and stand-off distance are considered the input layer during training. These parameters are distinct and recognized as four input neurons. The database was constructed by considering individual parameters across a range. Actual test data sets were utilized to train the ANN. The database was classified into three regions: (a) validation region, which describes the ANN architecture and accommodates neurons of a distinct layer, (b) a training region, useful for controlling the network weights, and (c) a testing region, relevant for data validation. Input parameters were normalized to the range 0 to 1. Approximately 27 data points were collected to train the neural network. Several ANN structures (Input-Hidden-Output), together with a variable quantity of neurons in the hidden layer, were examined for a fixed cycle, learning rate, error tolerance, momentum parameter, noise factor, and slope parameter. Depending on the minimum number of errors selected, the structure displayed in Table 3 was chosen for training the input-output data. The network optimization process (training and testing) was conducted over 2,000,000 cycles, over which error stabilization was achieved. Neuron numbers in the hidden layer were varied and, in the optimized network, found to be 12. The number of cycles selected during training was high enough for rigorous training of the ANN models. Just NN software was used, programmed with a back propagation algorithm, to apply the approach for predicting sample erosion in various test situations. The three-layer neural network with an input layer incorporating 4 input nodes, a hidden layer with 12 neurons, and an output layer with 1 output node is shown in Figure 3.

2.7. Signal-to-Noise (S/N) Ratio. The Taguchi concept emphasizes mathematical modeling to reduce time-consumption of experiments and testing by considering parametric optimization when estimating stable erosion under reasonable factors. Detailed explanation and clarification of controllable experiments to identify the ideal considerations in the DOE (design of experiment) is an effective analysis process. The choice of control and fixed parameters is important in DOE, and, in this respect, a large number of factors are incorporated to identify less important

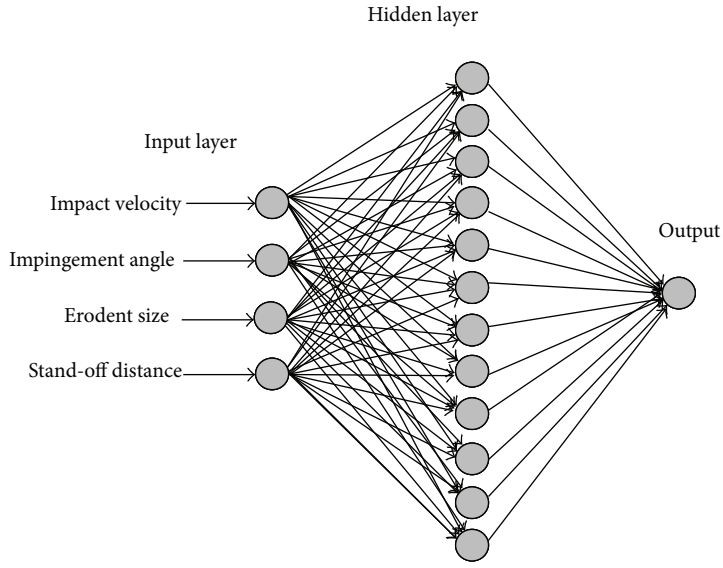

Figure 3: ANN concept viewing three layers.

Table 4: Parameters of the setting.

Fixed parameters	Fixed conditions/values	Control factor	Symbols
Nozzle diameter (mm)	5	Velocity of impact	*A*
Length of nozzle (mm)	55	Angle of impingement	*B*
Erodent	Silica sand under dry condition	Erodent size	*C*
Erodent shape	Irregular	Stand-off distance	*D*
Test temperature	Room temperature		
Erodent feed rate gm/sec	4.56		
Erodent microhardness (HV)	42–44		

variables as early as possible. In previous studies, erosion of polymers and composites was mainly dependent on the impingement velocity; controlling and constant factors are listed in Table 4. Considering the L27 (4^3) orthogonal array design concept, the significance of four variable factors at four different stages are designated.

The first column indicates variable parameters and the corresponding rows show the experimental conditions expressed in Table 5 as a blending of parameter levels. Four variable factors at four stages produce $4^3 = 64$ runs in a full factorial experiment. On the other hand, Taguchi's factorial technique minimizes it to 27 runs, providing a better representation of the results.

The number of tests is characterized as a S/N (signal-to-noise) ratio, of which several versions exist based on the type of characteristics. The analyzed ratio related to small amounts of erosive damage in the case of smaller is the better characteristic. Using this approach, this is determined as a logarithmic formulation of the loss function as follows.

In the case of less being the improved quality characteristic, this can be estimated using the following formula:

$$\frac{S}{N} = -10 \log \frac{1}{n} \left(\sum y^2 \right), \tag{3}$$

Table 5: Levels for various control factors.

Control factor	Level			Units
	I	II	III	
1*A*: velocity of impact	30	40	50	(m/s)
2*B*: angle of impingement	30	60	90	(Deg)
3*C*: erodent size	300–355	355–500	500–600	(μm)
4*D*: stand-off distance	15	20	25	(mm)

where n is the number of observations and y is the observed data. Less is regarded as the improved characteristic with respect to the S/N ratio transformation and is suitable for reducing the erosion rate. The design of the experiment is shown in Table 6, where the second, third, fourth, and fifth columns are designated as impact velocity (1*A*), impingement angle (2*B*), erodent size (3*C*), and stand-off distance (4*D*), respectively.

3. Results and Discussion

3.1. Influence of Impact Velocity. In erosion, the impingement velocity is related to the sustainability of the material's life. The test conditions were randomly shaped sand of dimension 300–355, 355–500, and 500–600 μm, stand-off distance

Table 6: Orthogonal array for L_{16} (4^4) Taguchi design.

L_{27} (4^3)	1*A*	2*B*	3*C*	4*D*
1	1	1	1	1
2	1	1	2	2
3	1	1	3	3
4	1	2	1	2
5	1	2	2	3
6	1	2	3	1
7	1	3	1	3
8	1	3	2	1
9	1	3	3	2
10	2	1	1	2
11	2	1	2	3
12	2	1	3	1
13	2	2	1	3
14	2	2	2	1
15	2	2	3	2
16	2	3	1	1
17	2	3	2	2
18	2	3	3	3
19	3	1	1	3
20	3	1	2	1
21	3	1	3	2
22	3	2	1	1
23	3	2	2	2
24	3	2	3	3
25	3	3	1	2
26	3	3	2	3
27	3	3	3	1

15 mm, and impingement angles 15, 30, and 60 degrees at ambient temperature. Under these test environments, erosion rates showed a sharp, increasing trend, with increases in velocity ranging from 30 to 50 m/sec for the tested gunmetal (Figures 4(a), 4(b) and 4(c)). Particles created a high impact of kinetic energy at high velocities, resulting in higher impact effect and greater erosion. In fact, particles occupy tremendous impact of kinetic energy at large velocity causing higher level of impacting effect and results in greater amount of erosion rate. In addition to that with increased velocity the duration between impacts is reduced and energy of the particle is increased which causes higher level of mass loss [17]. At 60-degree impact angle, the kinetic energies of 2052, 2793, 3648, 4617, and 5700 kg-m/sec were estimated for impact velocities of 30, 35, 40, 45, and 50 m/sec, respectively. Temperature variations were propagated throughout the sample surface with increasing velocities. However, due the effect of air-cooling during impaction by the compressor, the temperature increase is small. Nguyen et al. [18], Jha et al. [19], and ElTobgy et al. [20] reported a similar relationship between impingement velocity and erosion rate. Extended thermal characteristics have been observed at high velocities. Temperatures were elevated above ambient temperature level from 8 to 19 degrees for velocity increases between 30 and 50 m/sec. The increase in temperature may, in reality, be small due to rapid displacement of sand from the point of impact as well as cooling from the compressed pressure.

Table 7: The power law calculated values at different impingement angles.

Tested material	Impingement angle (α, °)	k	n	R^2
Gunmetal	15	0.007346	0.7841	0.99
	30	0.007340	0.7804	0.99
	60	0.004123	0.9130	0.99

The least-squares fitting of actual data was conducted by applying the power law. Consequently, erodent particle velocities of 30 m/sec, 40 m/sec, and 50 m/sec at impingement angles of 15°, 30°, and 60° were taken in to consideration for these purposes.

The relationship between stable erosive wear rate (E) and impingement velocity is stated as a simple power function:

$$E = kv^n, \tag{4}$$

where n is the velocity exponent and k is the proportionality constant impact on the other parameters. The influence of impact velocity on erosion rate of metals and alloys has been partially investigated. The velocity exponent (n) in general varies from 2 to 3 and 3 to 5 which indicate that the materials are ductile and brittle in nature, respectively [21]. The other mechanical properties (hardness, ultimate tensile strength, modulus of elasticity, fracture toughness, yield stress, yield strain, rebound resilience, etc.) can be correlated in this way.

The fitting parameters are listed in Table 7 and as an example the criteria of fitting calculation is expressed in Figures 5(a), 5(b), and 5(c) using GRAPHWIN software. Using the experimental data, calculated velocity exponents are obtained in the range of 0.78–0.91 for gunmetal at different impingement angle. This means that the findings of velocity exponents are found to be much lower than what have been mentioned by the different researchers for conformity of ductile behavior of tested material. In fact, the interesting observation in this study is that, in spite of the fact that the standard range for ductile material is within 2 to 3, it has been observed from the experimental data that the obtained velocity exponent range is true only for certain lower velocities and lower particle size. But at higher impact velocities, different erodent size, or particular shape of erodent, the velocity exponent can be found within the standard range. In this context, it can be realized that velocity exponent range varies with impact velocity, particular shape of erodent, and particle size. In case of coefficient of determination, relationship quality between erosion rate and impact velocity for exponential parameter is found to be stronger (99%) for test samples.

3.2. Influence of Impingement Angle. In order to study the effect of impingement angle on erosion rate, erosion tests were performed by varying the impact velocity from 30 to 50 m/s at impingement angles of 15° to 90° for different

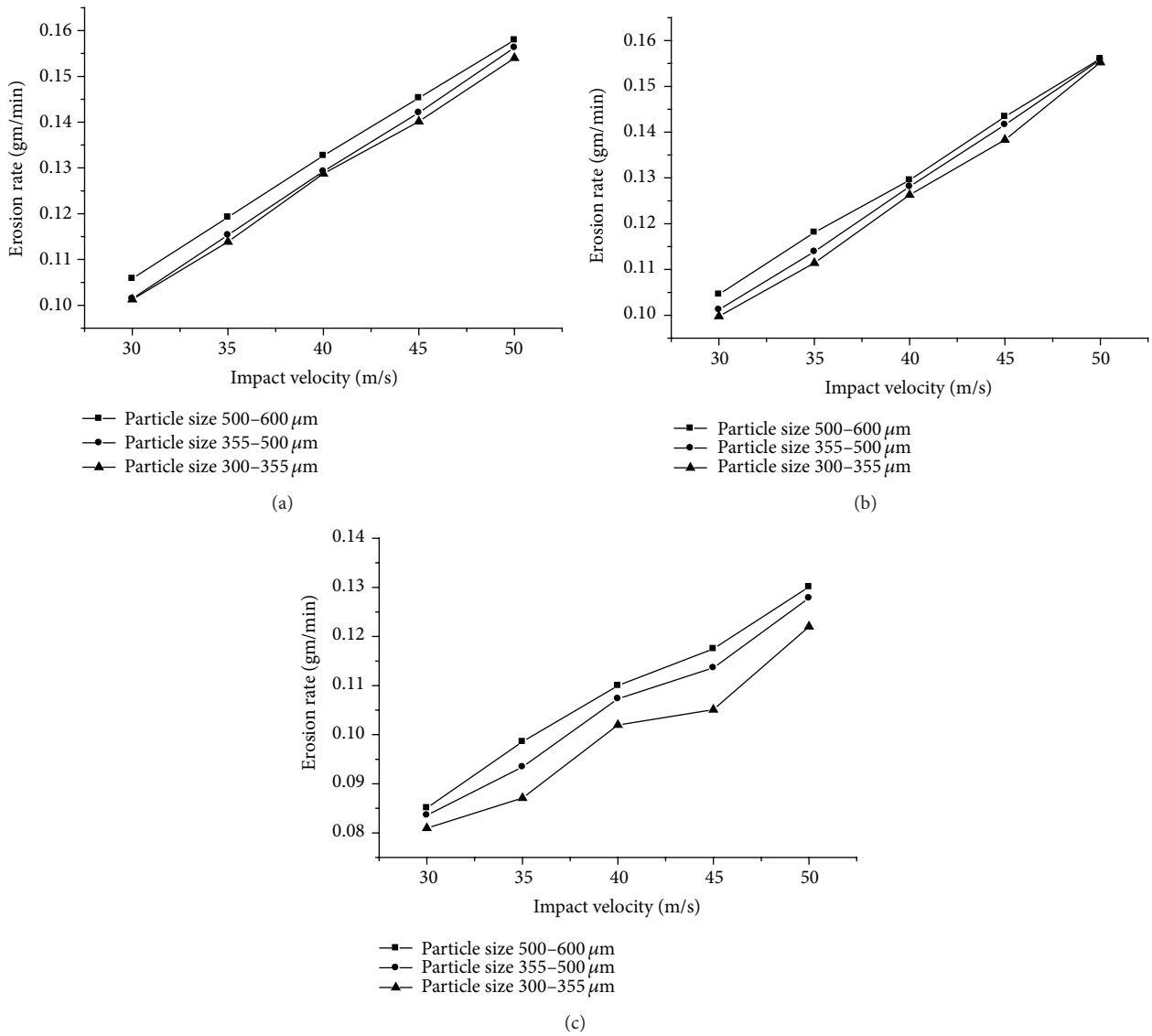

Figure 4: Variation of erosion rate with the variation of impact velocity and erodent size (impact angle: (a) 15 degrees, (b) 30 degrees, and (c) 60 degrees and stand-off distance 15 mm).

particle size. These results are presented in Figures 6(a), 6(b), and 6(c) showing the influence of impingement angle on the erosion rate of gunmetal at different impact velocities and particle size. It can be seen that erosion rate is maximum at 15° impingement angle for gunmetal at different impact velocities and particle size studied. At impact angle 15° erosion rates are high and then decrease gradually up to the impingement angle 45°. After that erosion rate increases ranging from 45° to 90°, in general, for all tested samples. The experimental results also show that erosion rates are slightly higher at 60° impingement angle in most cases as compared to 45°, 75°, and 90° impingement angle. It is known that impingement angle is one of the most important parameters for the erosion behavior of materials. In the erosion literature, materials are broadly classified as ductile or brittle, based on the dependence of their erosion rate on impingement angle. The behavior of ductile materials is characterized by maximum erosion rate at low impingement angles (15°–30°). Brittle materials, on the other hand, show maximum erosion under normal impingement angle (90°). Some materials have been shown, however, to exhibit a semiductile behavior with maximum erosion occurring in the angular range 45–60° [22–24]. However, the above classification is not absolute as the erosion behavior of metals and alloys but in reality it strongly depends upon the experimental conditions and mechanical and chemical properties of target materials. In the literature, there are no fixed trends of correlating ductility or brittleness of materials with α_{max} or α_{min}. It is found that some target materials are characterized in a ductile manner; on the other hand, some show evidence of both ductile and brittle characteristics [23, 25–27]. Nonferrous materials generally exhibit a more ductile response than ferrous materials [28]. The complexity of identifying the nature of alloys and metals as having ductile, semiductile, or

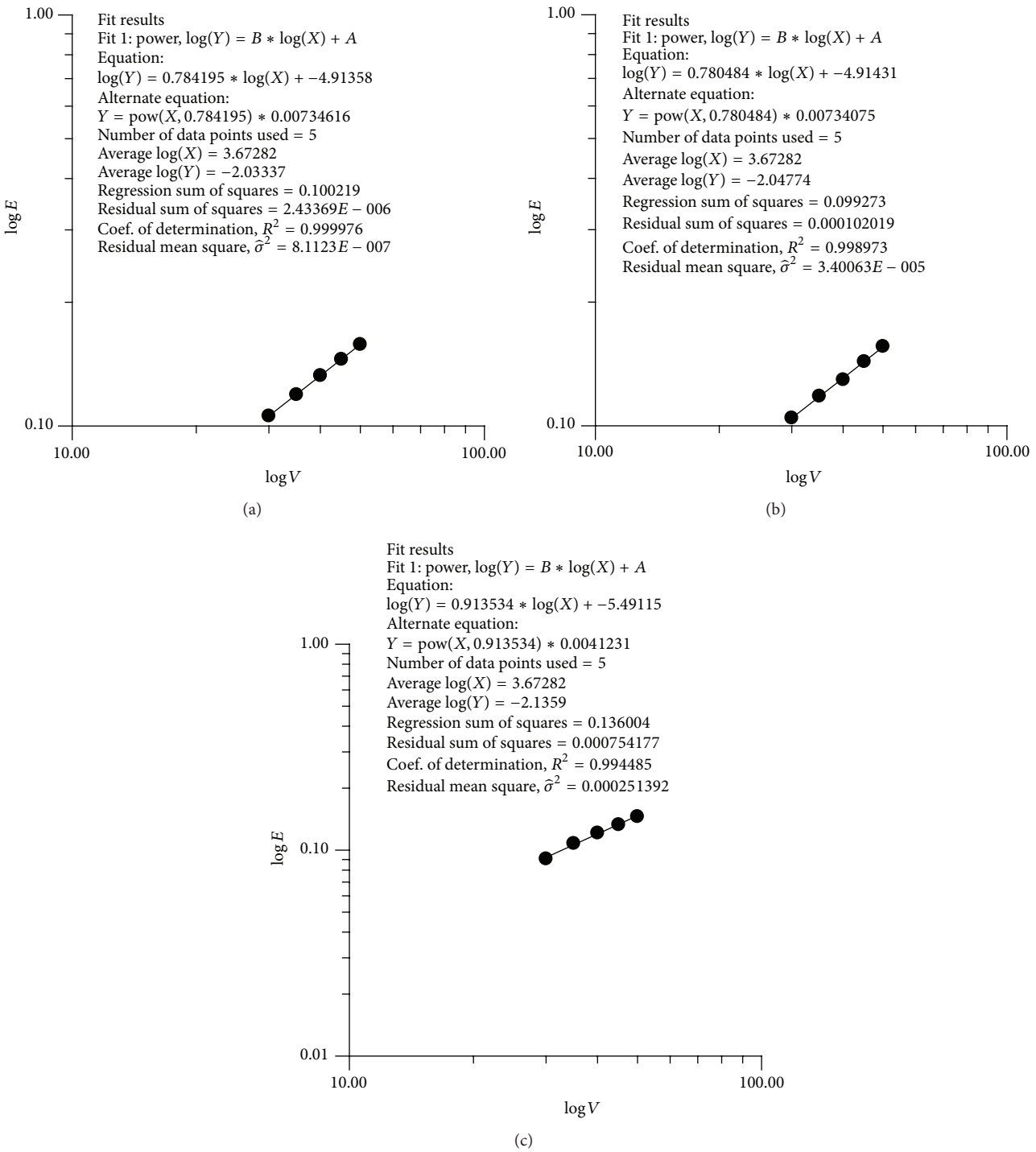

Figure 5: Curve fitting using power law equation for experimental data between erosion rate and impact velocity (test sample: gunmetal: (a) impact angle 15 degrees, (b) impact angle 30 degrees, and (c) impact angle 60 degrees and particle size 500–600).

brittle behavior makes it challenging for the researchers to summarize unique conclusion. As for example, Parslow et al. [29] reported that the maximum erosion rates are occurring at normal incidence for the copper based alloy and cast iron which ensured the brittle type erosion behavior. Thus, though the use of terms such as failure by "ductile," "semiductile," and "brittle" mechanisms is frequent and useful in understanding erosion of materials, it is not strictly true in all cases.

Generally, ductile characteristics are more sensitive to abrasive particles and the maximum erosion lies in the range of 15–30° as a result of microcutting, microploughing and other damage accumulation processes. For brittle materials,

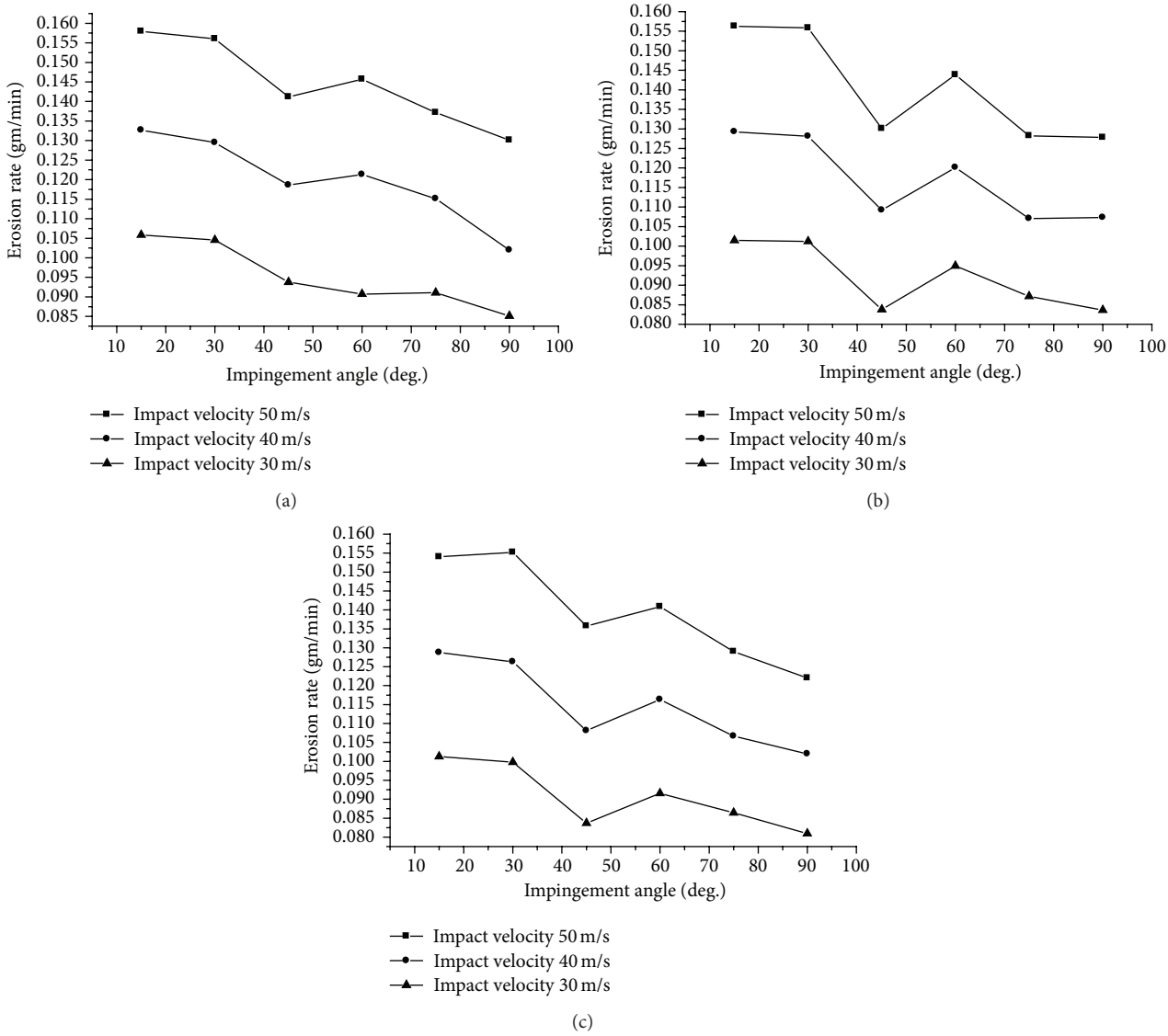

Figure 6: Variation of erosion rate with the variation of impingement angle ((a) particle size: 500–600 micron, (b) particle size: 500–600 micron, and (c) particle size: 500–600 micron and stand-off distance: 15 mm).

mechanisms like plastic deformation and microcracking are the responsible for erosion rate for that property. Depending on the impingement angle, cutting wear is dominant at acute angles while deformation wear is dominant at high impingement angles [30, 31]. It has been well accepted that maximum erosion for ductile material occurs at low angles between 15 and 30° where cutting mechanism dominates, while lower erosion rates are seen for high impingement angles where deformation wear occurs. The reverse is true for brittle material.

3.3. Significance of Particle Size on Erosion. Particle size has considerable effect on erosion of gunmetal under various impact velocities for 15-, 30-, and 60-degree impingement angle (Figures 7(a), 7(b), and 7(c)). The erosion rate of the tested material tended to increase with erodent size. Previous studies have emphasized the actual and analytical effects of erodent size when considering solid particle erosion of metals, alloys, polymers, and composites. Most results [32–36] show similar trends of erosive loss with respect to erodent size. Sundararajan and Roy [37], Mondal et al. [38], Dundar and Inal [39], and Lynn et al. [40] all performed erosion experiments using a wide range of particle sizes and observed that lower degrees of particle collision efficiency are responsible for reducing erosive wear with lower erodent sizes. They defined collision efficiency n as a ratio of the number of particles striking a unit area of the surface per unit time to the sum of particles incorporated within the volume of suspension swept by that area per unit time [41, 42]. Larger particles experience retardation just before impact due to the overinertial phenomenon. Therefore, their collision efficiency will be close to unity [29].

On the other hand, smaller particles are more susceptible to retardation before impact. Hence, their collision efficiency

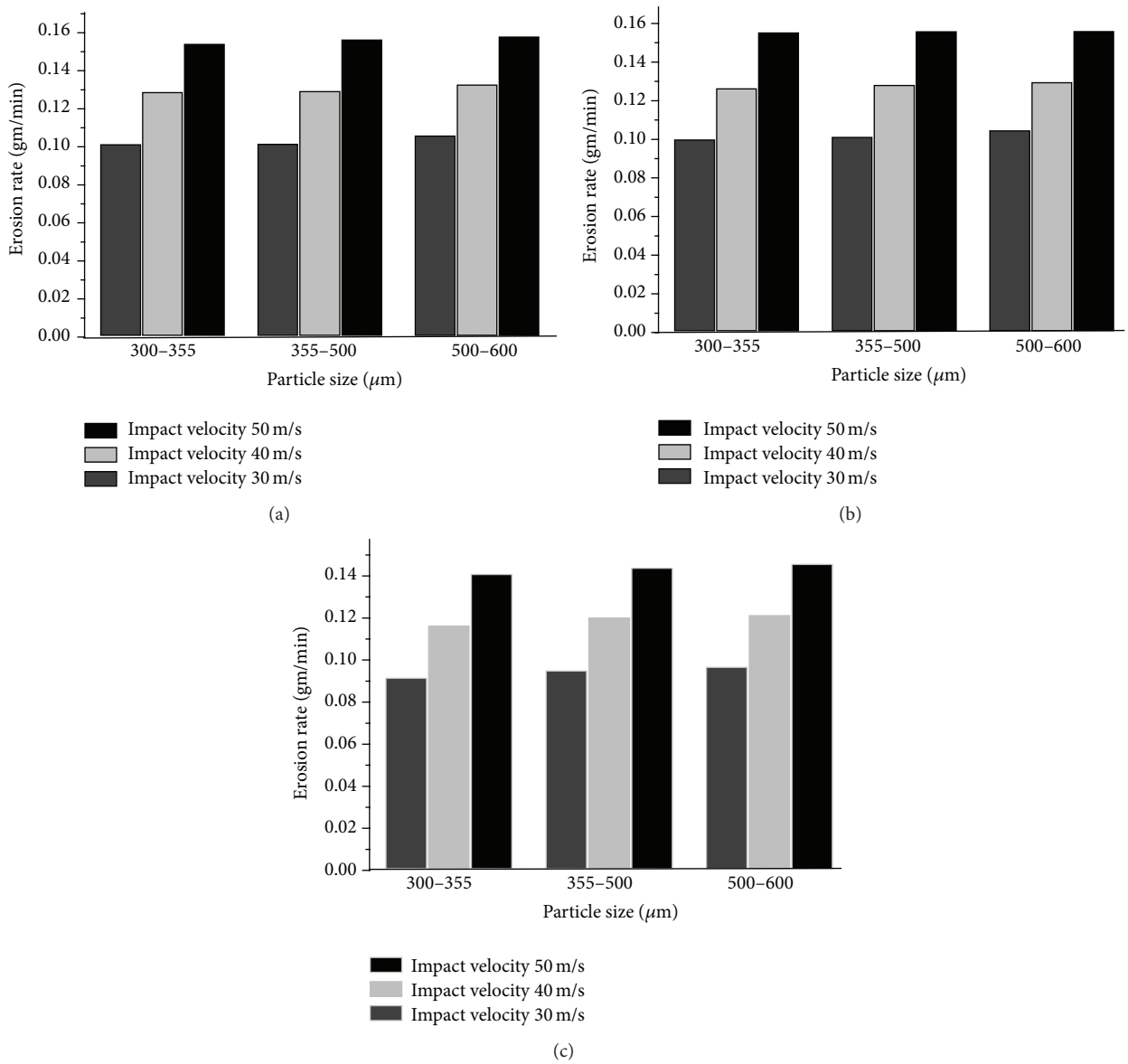

Figure 7: Bar chart showing erosion rate with different particle size ((a) impact angle: 15 degrees, (b) impact angle: 30 degrees, and (c) impact angle: 60 degrees and stand-off distance: 15 mm).

and kinetic energy dissipating after impact will be lower, causing a decrease in erosion rate. Several studies have shown that a higher erosion rate occurs with larger particle sizes due to higher energy transfer during impact from particle to target material. The increasing relationship between erosive wear and erodent size is associated with the following: (i) momentary enlargement of particle size and turbulent effect ensure a greater amount of particle striking force on the tested sample as a matter of propagation of indentation damage on the eroded surfaces under repeated action within a short period of time and (ii) in other cases the continuous sticking of expanded abrasive elements may deteriorate the subsurface and initiate fatigue-induced mass loss of surfaces. Generally, momentary particle action, indentation efficiency, and fatigue-initiated mechanisms are significant factors that influence increasing erosion with particle size [37]. In addition, there are some contradictory findings, with some results in practical test conditions showing that material erosion is not affected by particle size. The literature suggests that there may be an optimal level of particle size. The interplay of momentum of the erodent, indentation efficiency, and fatigue assisted erosive wear modes have also been reported by several other researchers.

3.4. Influence of Stand-Off Distance. We next examined the effect of the distance between the nozzle and target material on the erosion rate at impact angle 30°, impact velocity 40 m/sec, and three particle sizes. The variation in erosion rate with varying distance is shown in Figure 8. It can be seen that the reduction in erosive wear is related to increased

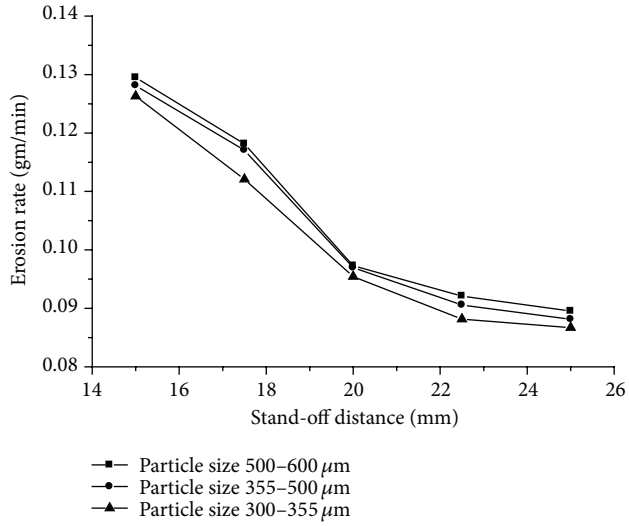

FIGURE 8: Erosion rate with different stand-off distance at different particle size (impingement angle: 30 degrees, impact velocity: 40 m/sec).

distance between nozzle and target material. This is due to the influence of kinetic energy and gravitational force of the sand particle reducing with increasing distance. In addition, when the nozzle and target material are relatively close to each other, particles may strike a small area of the test sample with a high concentration of particle flux but, in the case of large distance, particles may strike a large area of test sample with low concentrations of particle flux. At smaller distances, particles hit the surface as a beam but, with increasing distance, the strike area becomes V-shaped. The eroded impact areas for stand-off distance for 15, 17.5, 20, 22.5, and 25 mm were 63.24, 113.12, 141.47, 171.37, and 237.25 mm^2, respectively. In future studies, the concentration of particle flux in relation to stand-off distance should be measured.

3.5. Dimensional Analysis. Let

$$E_R = F\left(V, f, P, D\right), \tag{5}$$

where E_R is erosion rate, MT^{-1}, V is impact velocity, LT^{-1}, f is sand flow rate, MT^{-1}, P is particle size, L, and D is distance between nozzle and target material, L.

Let k be a dimensionless constant; then (5) can be written as follows:

$$E_R = k\left[V^a \cdot f^b \cdot P^c \cdot D^d\right]. \tag{6}$$

Substituting the dimensions of each physical quantity, (5) reduces to

$$\begin{aligned} MT^{-1} &= k\left[\left(LT^{-1}\right)^a \cdot \left(MT^{-1}\right)^b \cdot (L)^c \cdot (L)^d\right] \\ \text{or } MT^{-1} &= k\left[L^{a+c+d} \cdot T^{-a-b} \cdot M^b\right]. \end{aligned} \tag{7}$$

Since (5) must be dimensionally homogeneous, equate the powers of M, L, and T and obtain

$$\begin{aligned} b &= 1, \\ -a - b &= -1 \\ \text{or, } a &= 0 \\ a + c + d &= 0 \\ \text{or, } c &= -d. \end{aligned} \tag{8}$$

Therefore,

$$\begin{aligned} E_R &= k\left[V^0 \cdot f^1 \cdot P^{-d} \cdot D^d\right] \\ \text{or, } E_R &= kf\left[\frac{D}{P}\right]^d \\ \text{or, } E_R &= K\left[\frac{D}{P}\right]^d, \end{aligned} \tag{9}$$

where "d" and "K" are arbitrary constants.

The dimensional parameter D/P mentioned in (9) is designated the "Uttam Number" and can be expressed in brief as U. No.

The relationships between erosion wear (E_R) and U. No. for gunmetal under an impact velocity of 50 m/sec and impact angle 30° are displayed in Figure 9.

The curves show that erosion rate decreases linearly with increased U. No. and is represented by the following equation:

$$E_R = (0.142\text{–}0.794)\ \text{U. No. for gunmetal.} \tag{10}$$

In Figure 9, rectangular data points indicate the test observations of erosion rate with U. No. Using these actual data, least-squares equations and correlations were produced using ORIGIN software. The solid lines in the figure indicate trend lines. The correlation coefficient (r) was calculated to obtain −0.67614 for the test material. As a subjective measure of relationship between experimental data with trend line, the mentioned coefficient of correlation signifies that there are moderate negative relationships between erosion rate and Uttam Number. In this perception, it can be summarized that the actual data figure ensures acceptable recognition with the theoretical model.

Several models or correlations [11–16] have previously been proposed. Due to their complexity of application and rigorous mathematical procedures, our correlation indicates a simpler way to correlate erosion rate with U. No. using dimensional analysis. Previous and suggested correlations are listed in Table 8. In previous models, mechanical properties are given priority compared to the operating conditions. Our present method is novel in that it ensures the dependency of erosion rate with stand-off distance and particle size, which has not previously been taken into consideration.

3.6. Erosion Efficiency. The researchers [43] have established a formula for measuring erosion efficiency (η) mentioned in

$$\eta = \frac{2EH_v}{V^2 \rho \sin^2 \alpha}, \tag{11}$$

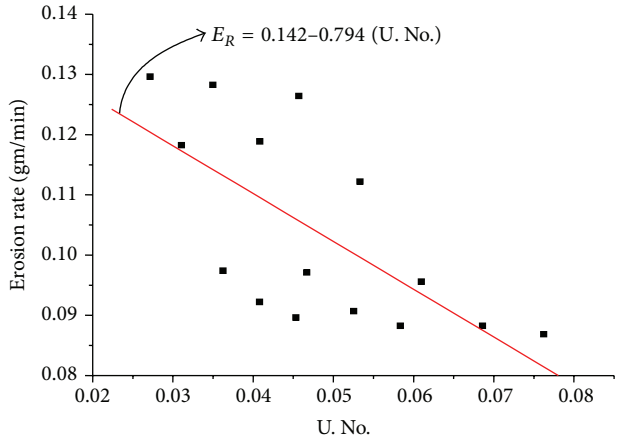

Linear regression data:
$Y = A + B * X$

Parameter	Value	Error	
A	0.14199	0.01197	
B	−0.79413	0.24	
R	SD	N	P
−0.67614	0.01245	15	0.00565

FIGURE 9: Erosion rate as function of U. No. for gunmetal.

where E is stable level of erosive wear, HV is the Vickers hardness of impacting element, V is impingement velocity, and ρ is the density of silica sand. Detachment of superficial layer in ideally microploughing effect on crater has been realized without initiation of fracture (indicates nonerosive nature) and signifies zero erosion efficiency. That is, ideally microcutting conditions are assumed to be unity. At the time of generation of erosive wear most likely as a lip and simultaneously the initiation of fracturing characteristics, η can be considered at the level of 0-1. Accordingly, for brittle material, when the erosive wear has been found due to material spelling as well as removal of higher level of chunks (due to interconnection of either lateral or radial cracking facts), in this case η can be assumed to be larger than 100%.

The hardness alone is unable to provide sufficient correlation with erosion rate, largely because it determines only the volume displaced by each impact and not really the volume of particle. Thus, a parameter which will reflect the efficiency with which the volume that is displaced is removed should be combined with hardness to obtain a better correlation. The erosion efficiency is obviously one such parameter. This thought has already been reflected in the theoretical model but the evaluation of erosion efficiency can be made only on the basis of experimental data. Hence, the values of erosion efficiencies of these alloy calculated using (6) are summarized in Table 9 along with their hardness values and operating conditions. The hardness values (H_v) and density (ρ) are 42, 43.2, and 44 MPa and 1436, 1440, and 1443 kg/m^3 of particle size 300–355, 355–500, and 500–600, respectively. It clearly shows that erosion efficiency is not exclusively a material property but also depends on other operational variables such as impingement angle and impact velocity. The erosion efficiencies of gunmetal under normal impact (η normal) vary from 3.58 to 25.07%, 4.55–33.78%, and 7.31–34.70% for impact velocities 50, 40, and 30 m/s, respectively. The value of η for a particular impact velocity under oblique impact can be obtained simply by multiplying a factor $1/\sin^2\alpha$ with η normal. Similar observation on velocity dependence of erosion efficiency has previously been reported by Arjula et al. [44]. The magnitude of η can be used to characterize the nature and mechanism of erosion. For example, ideal microploughing involving just the displacement of the material from the crater without any fracture (and hence no erosion) will result in $\eta = 0$. In contrast, if the material removal is by ideal microcutting, $\eta = 1.0$ or 100%. If erosion occurs by lip or platelet formation and their fracture by repeated impact, as is usually the case in the case of ductile materials, the magnitude of η will be very low; that is, $\eta \leq 100\%$. In the case of brittle materials, erosion occurs usually by sapling and removal of large chunks of materials resulting from the interlinking of lateral or radial cracks and thus η can be expected to be even greater than 100% [44]. According to the categorization made by this author, the erosion efficiencies of the composites under the present study indicate that at low impact speed the erosion response is semiductile ($\eta = 10$–100%). On the other hand at relatively higher impact velocity exhibits ductile ($\eta < 10\%$) erosion behavior.

3.7. Effect of Friction Coefficient. The experiments have shown that at the time of contact of high-velocity solid particles with the tested materials, the impact velocity is assumed to be generated in parallel and normal components (Figure 10). In fact, in this case, impact may cause some motion, and some resistance is assumed to be created due to the mechanical properties (such as hardness and tensile strength) of the target material. With this in mind, the friction coefficient was calculated in relation to the angle on theoretical grounds. Applying force analysis and bearing in mind frictional force (F) and tangential force (R), the friction coefficient can be calculated as follows:

$$F_X = F \sin\theta,$$
$$F = \frac{1}{2} m v^2, \tag{12}$$

where horizontal force $F_X = (1/2)mv^2 \sin\theta$ and vertical force are equal to reaction force

$$F_Y = R = \frac{1}{2} m v^2 \cos\theta. \tag{13}$$

We know that frictional force is equal to $F = \mu R$, $\mu = F/R$, or $\mu = \tan\theta$.

Friction coefficient calculated from the above equation and its corresponding erosion rate at 15–75-degree impact angles and impact velocity 50 m/sec are listed in Table 10.

In Figures 11, 12, and 13 rectangular scatter data show the experimental relationship between erosion rate and the friction coefficient. To justify the experimental relation with theoretical context, liner regression and correlation are developed by using ORIGIN software. Continuous lines shown in these figures indicate the polynomial regression

Table 8: Different models for erosion.

Model number	Equations describing the model	Constants of the model	Pair of materialswall, erodent
Model [11]	$V_{E_R} = \frac{m_p}{w_y}\frac{{u_p}^2}{k_s}\frac{1}{e}\left(\sin 2\alpha - \frac{6}{w_y}\sin\alpha^2\right)$	$e = 1.14$	Steel St4 san $k_s = 700$ MPa
Model [12]	$E_R = 278.90\left[\left(\frac{u_p}{100}\right)^{2.47}\cos\alpha^2\left(I - {e_t}^2\right) + 0.0832\left(\frac{u_p}{100}\right)^{2.344}\sin\alpha^2\left(I - {e_t}^2\right)\right]$		Steel 410, high silica sand
Model [13]	$M_c = \frac{\rho_t {u_p}^2 C m_p}{P\psi}\left[\sin 2\alpha - \frac{2\left(I + \left(m^p {r_p}^2/I_p\right)\right)}{w_y}\sin\alpha^2\right]$	$C = 0.015$ $w_y = 6$	Steel St4, sand
Model [14]	$E_R = K_A f(\alpha)\left(u_p\cos\alpha\right)^2\left(I - {R_T}^2\right) + f\left(V_{IN}\right)$	$K_A = 3.67 * 10^{-6}$	Steel 355, high silica sand
Model [15]	$E_R = A{u_p}^n f(\alpha)$ $f(\alpha) = b\alpha^2 + c\alpha$ Now $\alpha \le \alpha_0$	$\alpha_0 = 15^\circ$	Carbon steel, high silica sand
Model 0 [16]	$E_{R_v} = 0.00000163\left(u_p\cos\alpha\right)^{2.5}\sin\left(\frac{\alpha\pi}{45.4^\circ}\right) + 0.000000468\left(u_p\sin\alpha\right)^{2.5}$ Now $\alpha \le 22.7^\circ$		Carbon steel, coal dust
Model	$E_R = (0.142–0.794)$ U. No., where U $= D/P$		Gunmetal

Table 9: Erosion efficiency of different operating conditions for gunmetal (experimental design using L_{27} orthogonal array for Taguchi method analysis).

Exp. number	Impact velocity (m/s)	Density of impact particle (ρ) kg/m^3	Hardness of impact particle (H_v) MPa	Erosion rate (E_R) mg/kg	Erosion efficiency (η)
1	30	1436	42.00	1687.833	34.70975
2	30	1440	43.20	1298.000	33.62469
3	30	1443	44.00	1238.000	30.32633
4	30	1436	42.00	1172.167	9.855353
5	30	1440	43.20	1105.500	13.69071
6	30	1443	44.00	1512.000	8.261464
7	30	1436	42.00	957.833	9.316994
8	30	1440	43.20	1393.667	7.317492
9	30	1443	44.00	1077.667	10.53423
10	40	1436	42.00	1628.667	22.58272
11	40	1440	43.20	1501.333	33.78172
12	40	1443	44.00	2211.167	4.330798
13	40	1436	42.00	297.587	10.04006
14	40	1440	43.20	2002.167	7.844489
15	40	1443	44.00	1540.167	8.246998
16	40	1436	42.00	1699.833	5.106057
17	40	1440	43.20	1357.833	4.556597
18	40	1443	44.00	1193.000	6.517931
19	50	1436	42.00	1791.500	25.07766
20	50	1440	43.20	2605.000	19.85867
21	50	1443	44.00	2031.000	21.86445
22	50	1436	42.00	2347.500	5.924445
23	50	1440	43.20	1846.000	5.523551
24	50	1443	44.00	1694.500	4.961363
25	50	1436	42.00	1597.833	3.588368
26	50	1440	43.20	1491.000	5.301186
27	50	1443	44.00	2168.667	5.278079

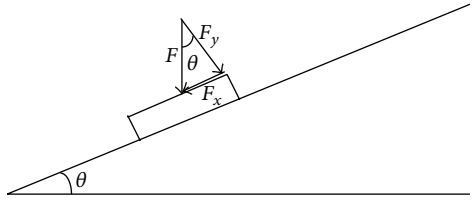

Figure 10: Impact velocity in parallel and normal directions.

Table 10: Friction coefficient and corresponding erosion rate at impact velocity 50 m/sec.

Impingement angle (degree)	Friction coefficient	Corresponding erosion rate at impact velocity 50 m/sec
15	0.268	0.15794
30	0.577	0.15602
45	1	0.14119
60	1.732	0.14569
75	3.732	0.13715

lines. The correlation coefficients are 0.778, 0.820, and 0.9296 for gunmetal, respectively, indicating strong positive relationships between erosion rate and friction coefficients for gunmetal. The experimental and theoretical data and are correlated to an acceptable level.

3.8. Steady State Erosion of Gunmetal. In Table 11, the first, second, third, fourth, fifth, and sixth columns represent impact velocity, impingement angle, particle size, stand-off distance, erosive wear, and S/N ratio, respectively. S/N ratio in context of erosive wear rate definitely indicates the arithmetic mean of two replications. Considering all S/N ratio of the erosive wear rate, the average level of the entire mentioned S/N ratio is calculated as −63.388 dB. Figure 14 shows the graphical presentation of main effect plot of S/N ratio emphasizing the consequence of the four varying

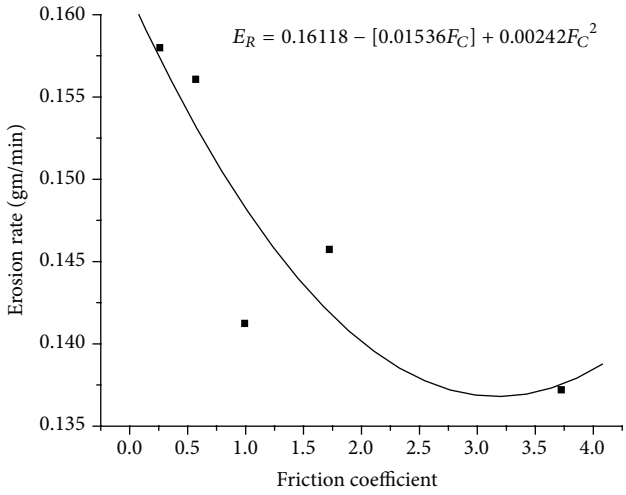

Polynomial regression for data1_B:
$Y = A + B1 * X + B2 * X^2$

Parameter	Value	Error
A	0.16118	0.00706
$B1$	−0.01536	0.01013
$B2$	0.00242	0.00239

R^2 (COD)	SD	N	P
0.77811	0.00607	5	0.22189

Figure 11: Erosion rate as function of friction coefficient (F_C) for gunmetal at impact velocity 50 m/sec.

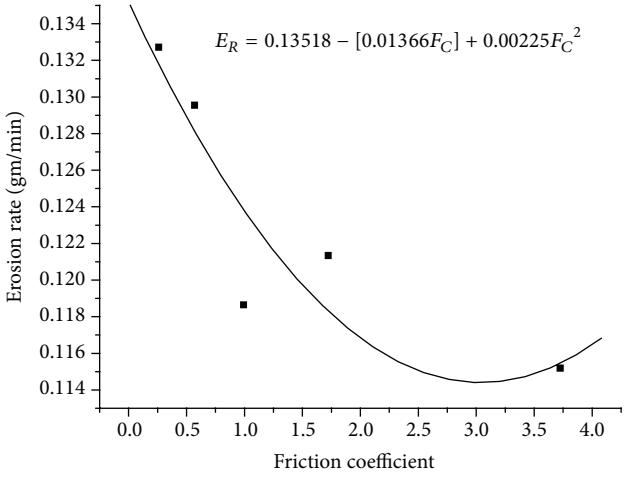

Polynomial regression for data3_B:
$Y = A + B1 * X + B2 * X^2$

Parameter	Value	Error
A	0.13518	0.00516
$B1$	−0.01366	0.00739
$B2$	0.00225	0.00175

R^2 (COD)	SD	N	P
0.82058	0.00443	5	0.17942

Figure 12: Erosion rate as function of friction coefficient (F_C) for gunmetal at impact velocity 40 m/sec.

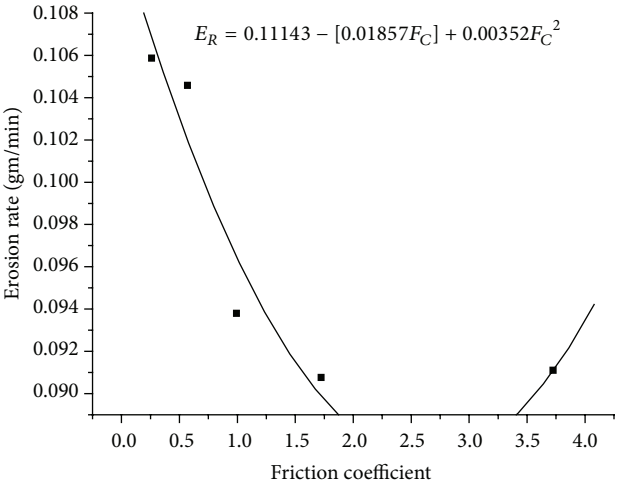

Polynomial regression for data4_B:
$Y = A + B1 * X + B2 * X^2$

Parameter	Value	Error
A	0.11143	0.00324
$B1$	−0.01857	0.00464
$B2$	0.00352	0.0011

R^2 (COD)	SD	N	P
0.92961	0.00278	5	0.07039

Figure 13: Erosion rate as function of friction coefficient (F_C) for gunmetal at impact velocity 30 m/sec.

parameters on erosive wear rate. MINITAB 15 software basically applicable for designing of experimental applicability is employed to analyze the results. This uncomplicated model is needed to predict the performance measurement; in relation to that the probable interrelations among the variable parameters are identified. Under this perception, factorial reflection integrating in an easier manner demonstrates the interaction effects. Analysis of test outcomes is used to make interpretation among the factor combination of $A1$, $B3$, $C1$, and $D3$, which contributes to evaluate the least amount of erosive wear rate.

Thus, factorial design incorporates a simple means of testing for the presence of the interaction effects. Analysis of the result leads to the conclusion that factor combination of $A1$, $B3$, $C1$, and $D3$ gives minimum erosion rate. The interaction graphs are shown in Figures 15(a), 15(b), and 15(c). As far as minimization of erosion rate is concerned, factors A, B, C, and D have significant effect. It is observed from Figure 15(b) that the interaction in $A \times C$ shows most significant effect on erosion rate. But the factors A and B individually have greater contribution on output performance, and their combination of interaction with factors A and B is shown in Figure 15(a) and has less effect on erosion rate and the factors B and C individually have greater contribution on output performance, and their combination of interaction with factors B and C is shown in Figure 15(c) and has less effect on erosion rate and then can be neglected for further study.

Table 11: Variation of erosion rate with different operating conditions for gunmetal (experimental design using L_{27} orthogonal array for Taguchi method analysis).

Exp. number	Impact velocity 1*A* (m/s)	Impingement angle 2*B* (degree)	Particle size 3*C* (μm)	Stand-off distance 4*D* (mm)	Erosion rate (E_R) mg/kg	S/N ratio (dB)
1	30	30	300–355	15	1687.833	−64.5466
2	30	30	355–500	20	1298.000	−62.2655
3	30	30	500–600	25	1238.000	−61.8544
4	30	60	300–355	20	1172.167	−61.3798
5	30	60	355–500	25	1105.500	−60.8712
6	30	60	500–600	15	1512.000	−63.591
7	30	90	300–355	25	957.833	−59.6258
8	30	90	355–500	15	1393.667	−62.8832
9	30	90	500–600	20	1077.667	−60.6497
10	40	30	300–355	20	1628.667	−64.2366
11	40	30	355–500	25	1501.333	−63.5295
12	40	30	500–600	15	2211.167	−66.8924
13	40	60	300–355	25	297.587	−49.4723
14	40	60	355–500	15	2002.167	−66.03
15	40	60	500–600	20	1540.167	−63.7514
16	40	90	300–355	15	1699.833	−64.6081
17	40	90	355–500	20	1357.833	−62.6569
18	40	90	500–600	25	1193.000	−61.5328
19	50	30	300–355	25	1791.500	−65.0643
20	50	30	355–500	15	2605.000	−68.3162
21	50	30	500–600	20	2031.000	−66.1542
22	50	60	300–355	15	2347.500	−67.4121
23	50	60	355–500	20	1846.000	−65.3246
24	50	60	500–600	25	1694.500	−64.5808
25	50	90	300–355	20	1597.833	−64.0706
26	50	90	355–500	25	1491.000	−63.4696
27	50	90	500–600	15	2168.667	−66.7239

Figure 16 shows the combination factor of erosion rate with impact velocity and impingement angle. It can clearly be seen that erosion rate increases with increased impact velocity at impact angle 15° due to the maximum particle energy transfer to the tested sample surface and less deformation occurring at the eroded surfaces. Maximum microcutting and ploughing occur at 15-degree impingement angle. The contour plot between impact velocity and impingement angle, impact velocity and erodent size, and impact velocity and stand-off distance is shown in Figure 17, while Figure 18 shows the 3D relationship between erosion rate and impact velocity, impact angle, and standoff distance. Large amounts of material were transferred from the tested surface material due to the impact velocity of 46–48 m/sec at a distance of 22–24 mm. Erodent size is an important factor dictating solid particle erosion rate.

3.9. ANOVA and the Effects of Factors of Gunmetal. Analysis of variance (ANOVA) chart is a decision making methodology for exact confirmation of imagining the significance of effecting level of factors considered. In addition to that ANOVA is an analyzing tool to select the order of more meaningful factors. Table 12 signifies the analysis of ANOVA to realize the contribution of factors on erosive wear rate. The ANOVA with erosion rate results are listed in Table 12. This analysis was assumed to be considered for a level of significance of 5%, that is, for level of confidence 95%. The last column of the table indicates the order of significance among control factors and interactions. It can be realized from Table 12 that the control factor $P = 0.027$ has highest static influence of 28.81%, $P = 0.045$ has an influence of 22.29%, $P = 0.218$ has an influence of 8.10%, and $P = 0.345$ has an influence of 5.23% on erosive wear rate of tested

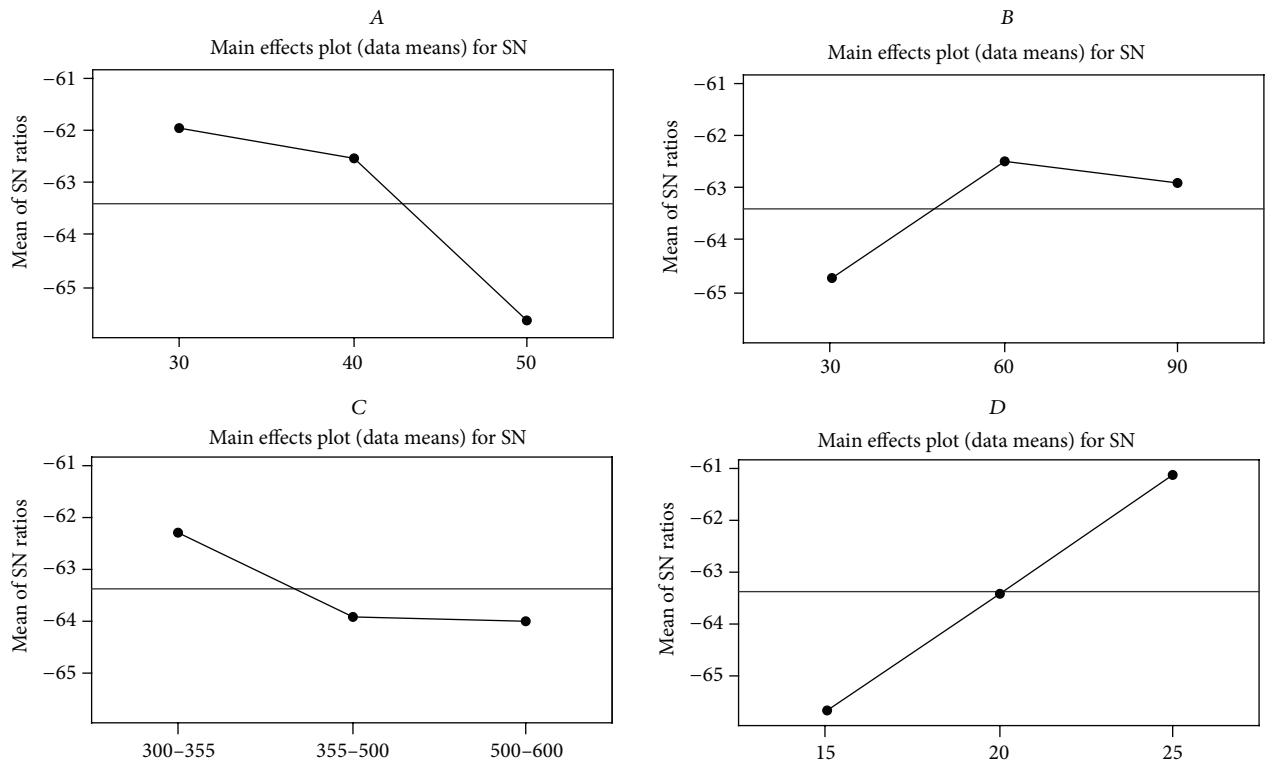

Figure 14: Effect of control factors on erosion rate of gunmetal.

Table 12: Effects of factors of gunmetal. Analysis of variance for S/N, using adjusted SS for tests.

Source	DF	Seq. SS	Adj. SS	Adj. MS	F	P	P (%)
A	2	72.266	72.266	36.133	5.45	0.045	22.29
B	2	26.275	26.275	13.137	1.98	0.218	8.10
C	2	16.948	16.948	8.474	1.28	0.345	5.23
D	2	93.402	93.402	46.701	7.04	0.027	28.81
$A * B$	4	23.756	23.756	5.939	0.90	0.521	7.33
$A * C$	4	26.060	26.060	6.515	0.98	0.482	8.04
$B * C$	4	25.747	25.747	6.437	0.97	0.487	7.94
Error	6	39.777	39.777	6.629			12
Total	26	324.231					

material system under observations. The results indicated that the factor (D) that is stand-off distance and impact velocity (A) exerted more effect on the erosion rate, followed by the impingement angle (B) and particle size (C). The effect of combined factors on impact velocity and sand size ($A * B$) on erosive wear performance played a crucial impact.

In case of comparative analysis of interaction of different alternative factors, $A * C$ = interaction within impingement velocity * erodent size ($P = 0.482$) has less number of P values compared to other two combinations. According to this perception, the factor interaction $A * B$ = velocity of impact * angle of impingement ($P = 0.521$) implies lesser significance of contribution on erosive wear rate in comparison with factor interaction $B * C$ = angle of impingement * erodent size ($P = 0.487$). Hence, the lower the P values, the higher the significance of contribution on the erosion rate justified. The present analysis shows that four levels of erosive test parameters impact velocity (A) and stand-off distance (D) individually and have both statistical and physical significance (percentage contribution is greater than error) in case of erosion rate of gunmetal. But interaction combinations between different control parameters have statistical significance but do not have physical significance, since error evaluated is more than percentage contribution of these interactions, which is evident from the ANOVA results.

3.10. Morphology of Eroded Surfaces

3.10.1. SEM Analysis

Surface Morphology at Different Impingement Angle. Then analysis of surface morphology of gunmetal was examined by using JEOL JSM 7600F Scanning Electron Microscope (country of origin Japan). SEM micrographs of eroded surfaces of gunmetal are appearing in Figures 19(a), 19(b), 19(c), 19(d), 19(e), and 19(f). Figures 19(a) and 19(b) specifies that gunmetal eroded surface at 15° impact angle is worn by the mechanism of microploughing, grooves, displaced material, and large fragments. Extensive ploughing and the resulting lip formation are evident in the micrograph for 15° impingement angle. The direction of ploughing in surface morphologies coincides with the direction of particle motion during sand blasting. This is the angle where the higher amount of erosion has been noted under all test conditions.

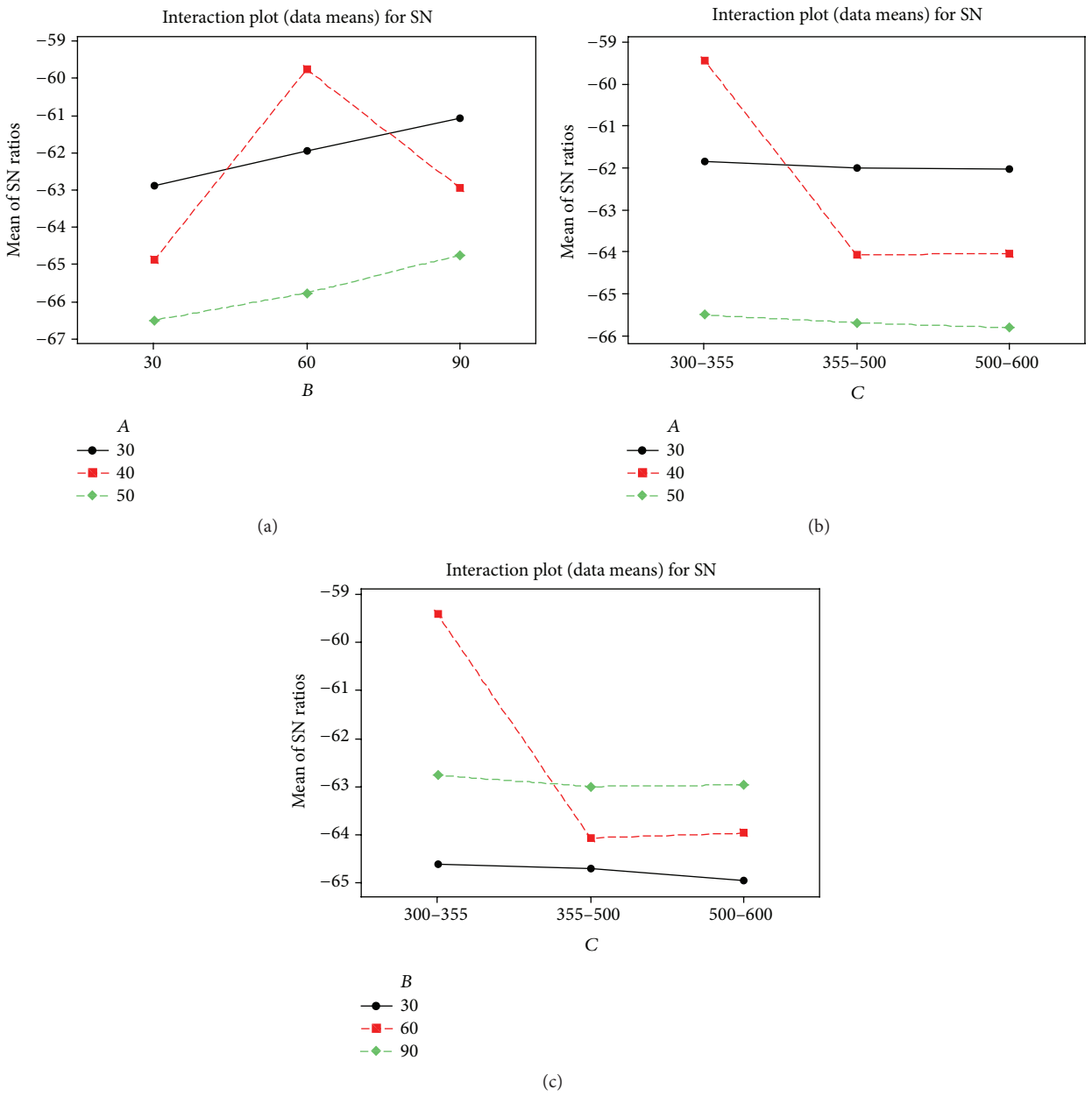

Figure 15: Interaction graph between (a) $A \times B$, (b) $A \times C$, and (c) $B \times C$ for erosion rate of gunmetal.

Materials which show ductile erosion behavior can be easily worn off by microploughing erosion mechanisms caused by the lateral impact of the particles. In Figures 19(c) and 19(d) at 30° impingement angle pitting action and craters have occurred as a result of lower erosion rate of the all tested materials. On the other hand at 60-degree impingement angle plastic deformation, craters, and microcutting action have occurred in Figures 19(e) and 19(f). The reduction in mass loss at higher impact angles, near or at 90° at velocity lower than 50 m/sec, is because there was not too much evidence of sliding action of abrasive particles unlike lower impact angles where the sliding component is significant and increases the mass lost in the material. But the reverse is true in few cases for high impact velocity 50 m/sec due to the quick impacting at short contact time between particle and target surface.

Surface Morphology with Different Impact Velocity. Surface morphology at different impact velocity has been presented in Figures 20(a), 20(b), 20(c), and 20(d) for analyzing the wear mechanism. Figures 20(e) and 20(f) under impact velocity 30 m/sec emphasized the lower erosion rate due to displaced material and putting action. This is because of the low particle energy. Figures 20(c) and 20(d) show that the damage has occurred on the target surface at impact velocity 40 m/sec. In this case the damaged has been done by the influence of craters, pulling action. At higher impact velocity (50 m/sec)

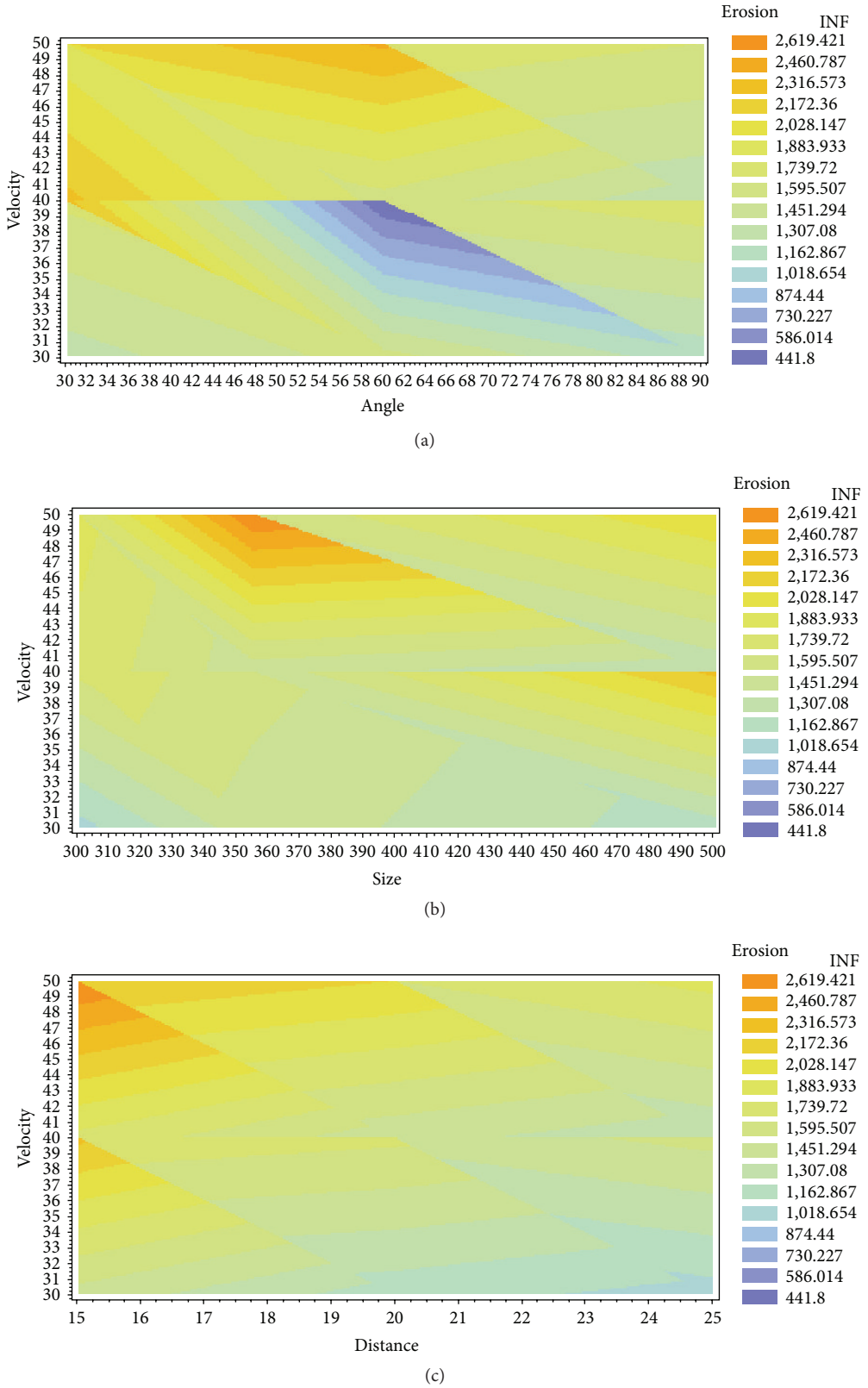

Figure 16: Heat map between (a) impact velocity and impingement angle, (b) impact velocity and erodent size, and (c) impact velocity and stand-off distance of gunmetal.

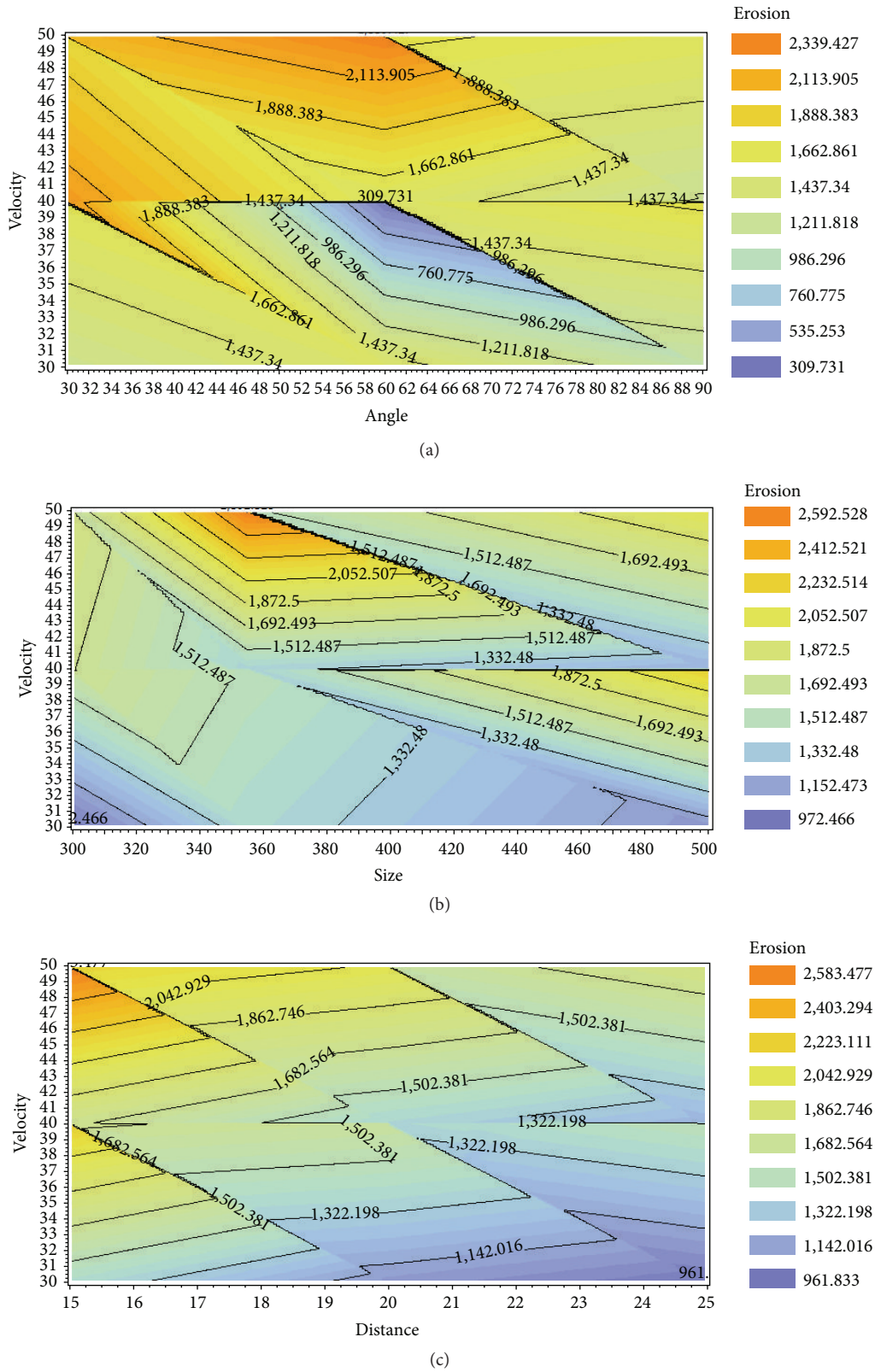

Figure 17: Contour plot between (a) impact velocity and impingement angle, (b) impact velocity and erodent size, and (c) impact velocity and stand-off distance of gunmetal.

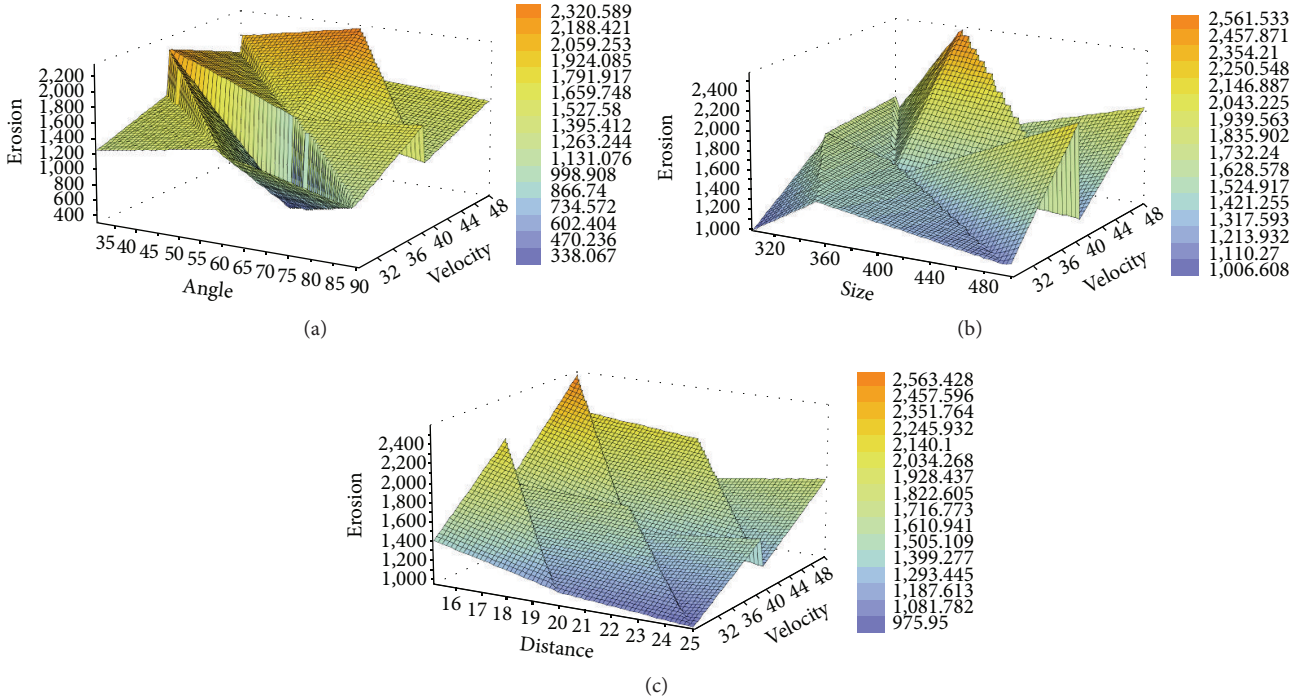

Figure 18: 3D Surface plot among erosion rate, impact velocity, impingement angle, and stand-off distance (a, b, c) for gunmetal.

due to the effect of crack and ploughing action, higher levels of erosion are obtained as a result of high particle energy (Figures 20(a) and 20(b)).

3.11. Analysis of Erosion with Different Percentage of Gunmetal at Different Impact Angles Using Energy Dispersed X-Ray Spectrograph (EDX). The analysis of energy dispersed X-ray spectrograph (EDX) of gunmetal was done by using JEOL JSM 7600F Scanning Electron Microscope (country of origin Japan). In this method an electron beam of 10–20 KeV strikes at the tested surface that causes X-ray to be emitted from the point of incidence. The emission energy of X-ray depends on the types of materials under observation; that is, the use of X-ray energy emission shows distinct nature depending on soft to hard materials and thus it gives the unavoidable signature in case of some kinds of materials. When an X-ray strikes the detector, it will generate a photoelectron which in turn generates electron hole pairs. A strong electric field attracts the electrons and holes towards the opposite ends of the detector. The size of the pulse thus generated depends on the number of electron hole pairs created, which in turn depends on the energy of the incoming X-ray. In this method however elements with low atomic number are difficult to be detected. The detector which is lithium doped silicon (SiLi) is protected by a beryllium window and operated at liquid nitrogen temperatures.

Figures 21 and 22 show the amount of silica embedded within the eroded surfaces at impact angle of 15 degrees. Similar observations are found in Figures 23, 24, 25, and 26 for impact angles of 60 and 90 degrees, respectively. The EDX analysis shows that the percentages of embedded silica are increased with the decrease of percentage of copper in gunmetal for all tested angles. The significance of these observations is that the higher the copper composition in gunmetal, the lower the silica engagement within the target surfaces which causes lower erosion rate. The depth at which the particle has been embedded into the material was very small depth from the upper surface. Just beneath the lip, the particle embedded into the material has been observed by other researchers as well [45]. It was assumed that the amount of fragmentation and secondary erosion would be dependent on the particle velocity, impingement angle, particle size, stand-off distance, and different in hardness between the particle and target material. The variation of composition of tin and zinc has some limited role with the variation of erosion rate.

The existence of the O and Si atoms in high percentage was the evidence of the embedded erodent garnet particles to the surfaces of the samples. Based upon the EDX analysis results, it was concluded that the erodent particles were embedded to the surfaces of the g during the erosion process. It was concluded that this can be possible because of the ductile behavior of the gunmetal.

3.12. Confirmation Experiment for Gunmetal. The end level of Taguchi approach is the validation of experimental observations for analyzing the quality characteristics. The validity of test results is ensured by concerning an arbitrary set of factor level combination and after that it has been compared with the test results. The measured S/N ratio for wear rates is estimated in connection with the predictive equations.

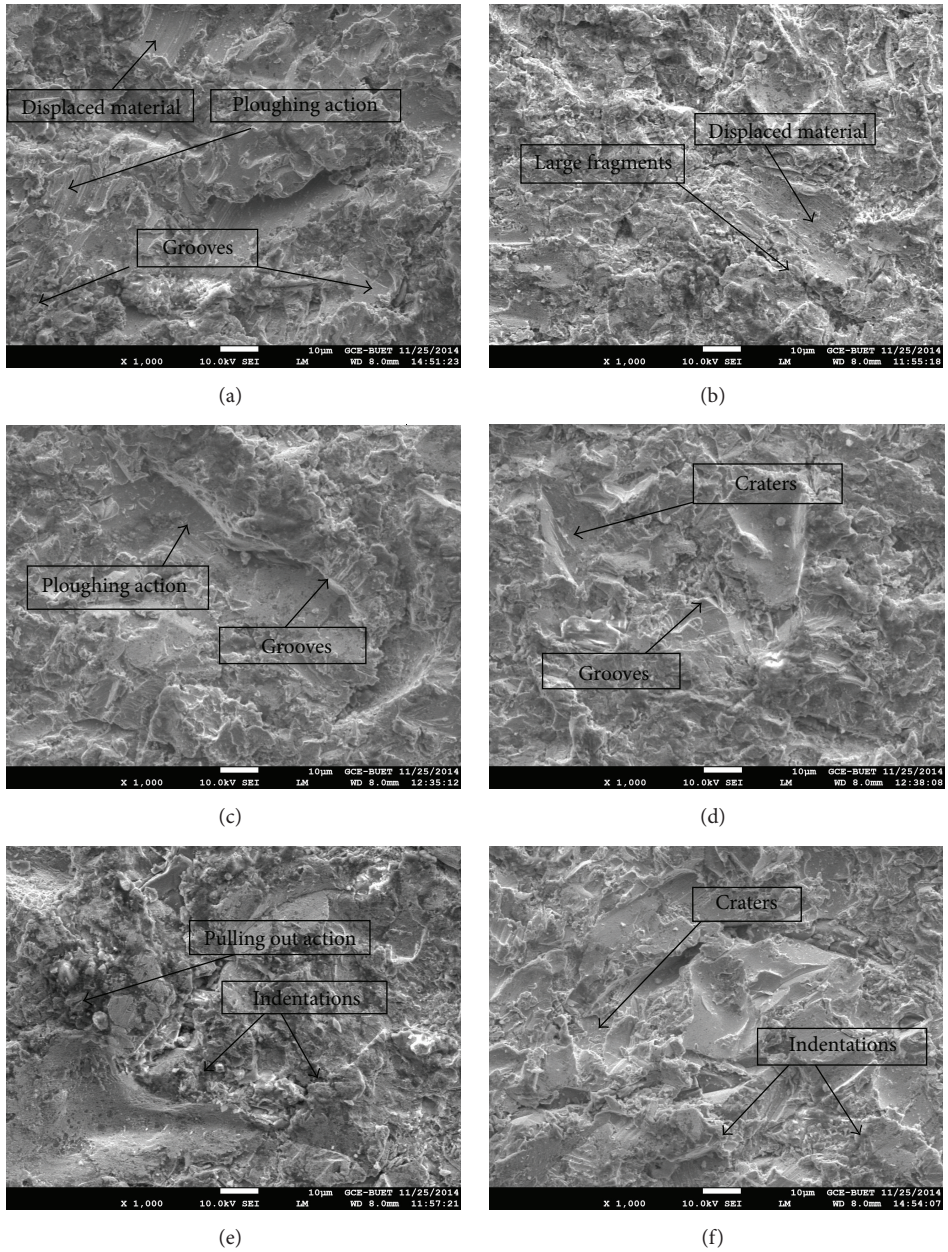

Figure 19: SEM micrograph of eroded aluminum alloy at impact angle, (a, b) 15 degrees, (c, d) 30 degrees, and (e, f) 60 degrees.

The estimated S/N ratio for wear rates can be calculated with the help of following predictive equations:

$$\overline{\eta} = \overline{T} + \left(\overline{A}_2 - \overline{T}\right) + \left(\overline{B}_3 - \overline{T}\right) + \left(\overline{C}_2 - \overline{T}\right) + \left(\overline{D}_1 - \overline{T}\right), \tag{14}$$

where $\overline{\eta}$ is the predicted average; $\overline{T}$ is overall experimental average; $\overline{A}_2$, $\overline{B}_3$, $\overline{C}_2$, and $\overline{D}_1$ are the mean response for factors at designated levels.

By combining like-terms, the equation reduces to

$$\overline{\eta} = \overline{A}_2 + \overline{B}_3 + \overline{C}_2 + \overline{D}_1 - 3\overline{T}. \tag{15}$$

A new combination of factor levels $A2$, $B3$, $C2$, and $D1$ is used to predict deposition rate through prediction equation and it is found to be $\overline{\eta} = -64.866$ for each performance measure; an experiment was conducted for different factors combination and compared with the result obtained from the predictive equation.

The new generated model is very meaningful for the prediction erosive wear rate to a justifiable accuracy. The calculated deviation (error level) is 1.72% and is obtained in case of S/N ratio of erosive wear rate. The results of experimental confirmation using optimal erosive wear parameters and comparison of the predicted erosion rate with the actual erosion rate using the optimal erosive wear parameters are

Table 13: Results of the confirmation experiments for erosion rate of gunmetal.

		Optimal control parameters		
	Initial process parameter	Prediction	Experimental	Improvement in the result
Level	$A2$, $B1$, $C2$, $D3$	$A2$, $B3$, $C2$, $D1$	$A2$, $B3$, $C2$, $D1$	
S/N ratio for erosion rate (dB)	−64.608	−64.866	−63.750	0.858
Erosion rate (mg/gm)	1699.83	1300.07	1523.80	10.35

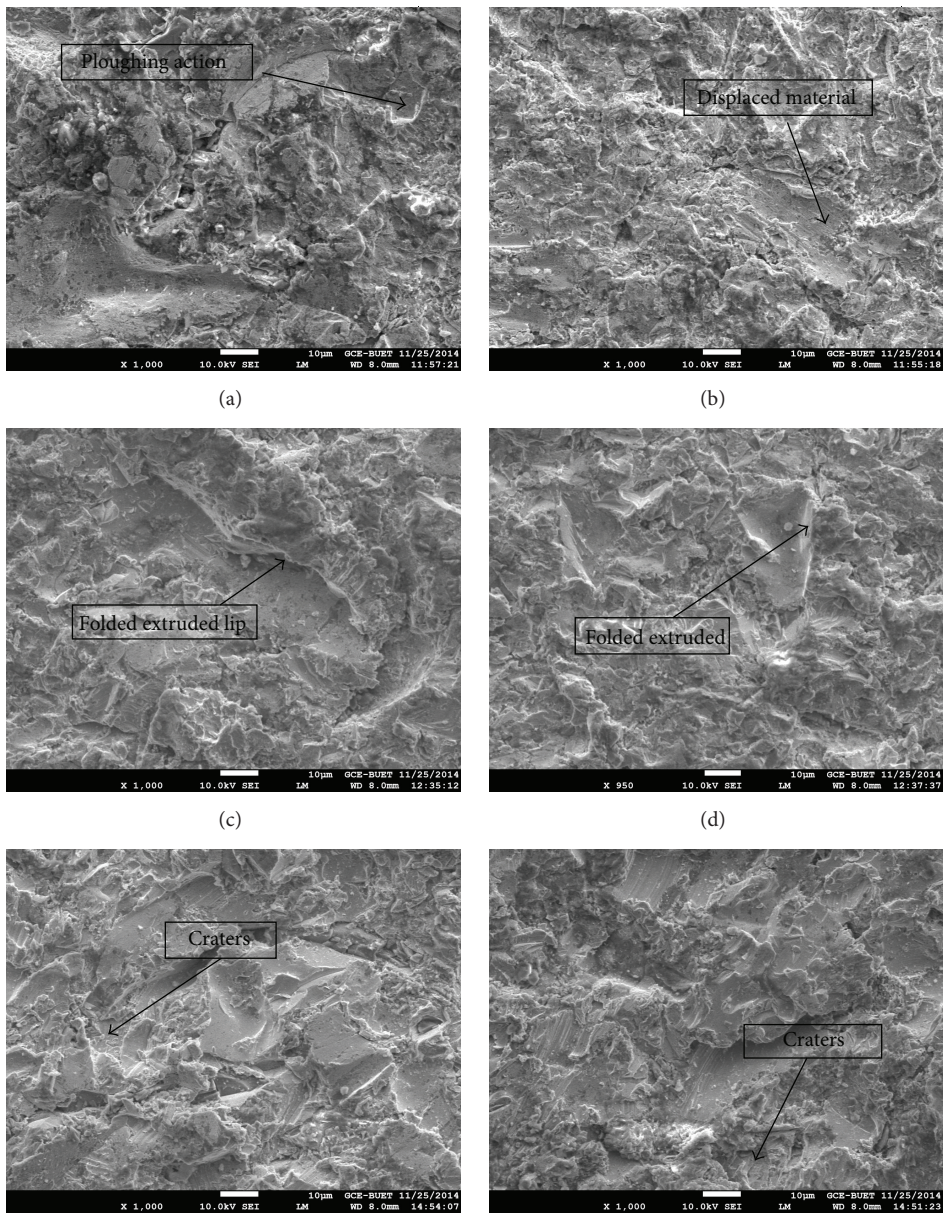

Figure 20: SEM micrograph of eroded gunmetal at impact velocity: (a, b) 50 m/sec, (c, d) 40 m/sec, and (e, f) 30 m/sec.

indicated in Table 13. The improvement in S/N ratio from the starting level to optimum level is 0.858 dB. The erosion rate is reduced by almost 10%. Considering this scientific approach, it can be mentioned that erosion rate performance is improved by using Taguchi method. After all, the accuracy level can be improved more precisely in case of increase of the number of measurements. This validation approach incorporates the generation of the mathematical model for the prediction of measures of performance on the basis of knowledge of the input parameters.

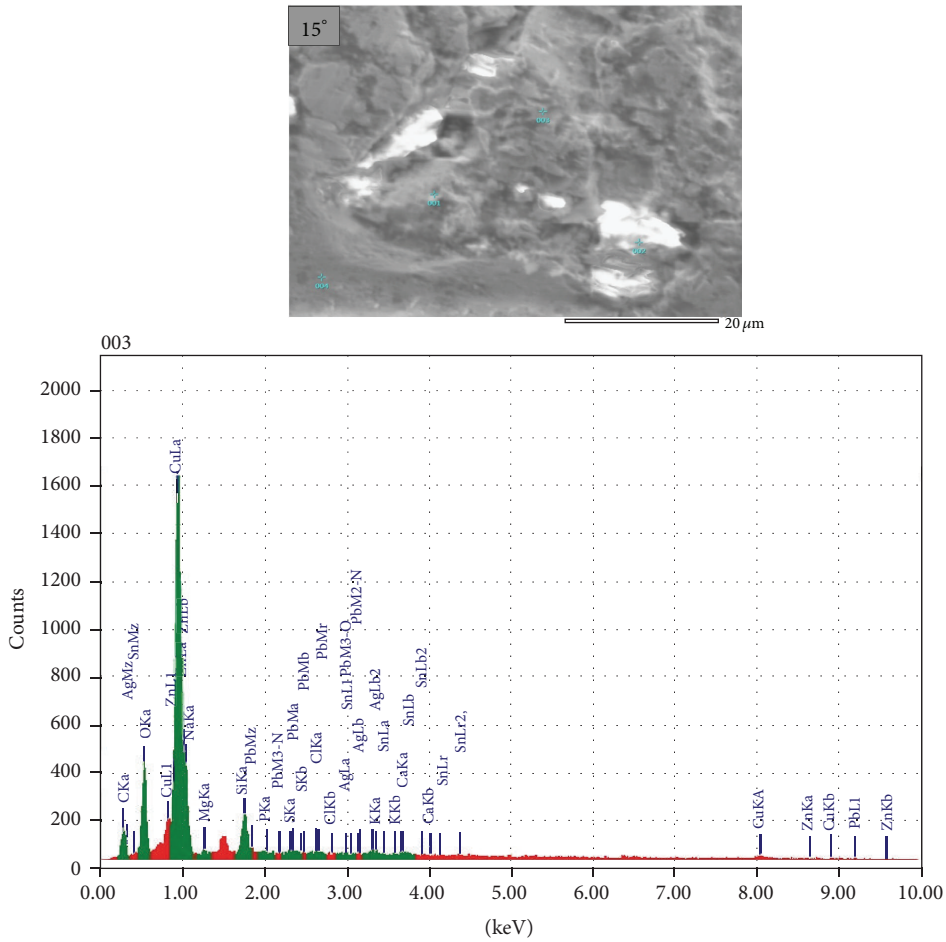

Element		(keV)	Mass (%)	Sigma	Atom (%)	Comp.
C K	*	0.277	14.47	3492109059358720	00.00	
O K		0.525	16.02	6406310683989770	20.00	
Na K	*	1.041	2.48	3062169432731156	50.00	
Mg K	*	1.253	0.46	1344336531858391	00.00	
Si K		1.739	4.59	4050316681690480	60.00	
P K						
S K	*	2.307	0.43	1237271844801740	80.00	
Cl K	*	2.621	0.20	9212594898757222	4.00	
K K	*	3.312	0.59	1961843822753218	60.00	
Ca K	*	3.690	0.55	2041432487325859	80.00	
Cu L	*	0.930	43.64	1109816800507330	600.00	
Zn L	*	1.012	16.15	9776320695070883	80.00	
Ag L	*					
Sn L	*	3.442	0.06	8141566635094835	2.00	
Pb M	*	2.342	0.36	1782626176204800	00.00	
Total			100.00		100.00	

Figure 21: Energy dispersed X-ray spectrograph (EDX) aluminum alloy at 15-degree impact angle.

4. Conclusions

The erosion results of gunmetal have provided some new findings relevant to different operating parameters. The validation of results and correlation of erosion with friction, Uttam Number, artificial neural network, ANOVA, erosion efficiency, S/N ratio methodology, GMDH concept have made the realization of novelty of the erosion study of this gunmetal. The morphological analysis provides the evidence of real wear mechanism incorporating displaced materials, grooves, ploughing action, large fragment, pitting action, indentations, crack, folded extruded lip, wear debris, and other related concerning issues for the eroded surface characterization under different impact angles, impact velocity,

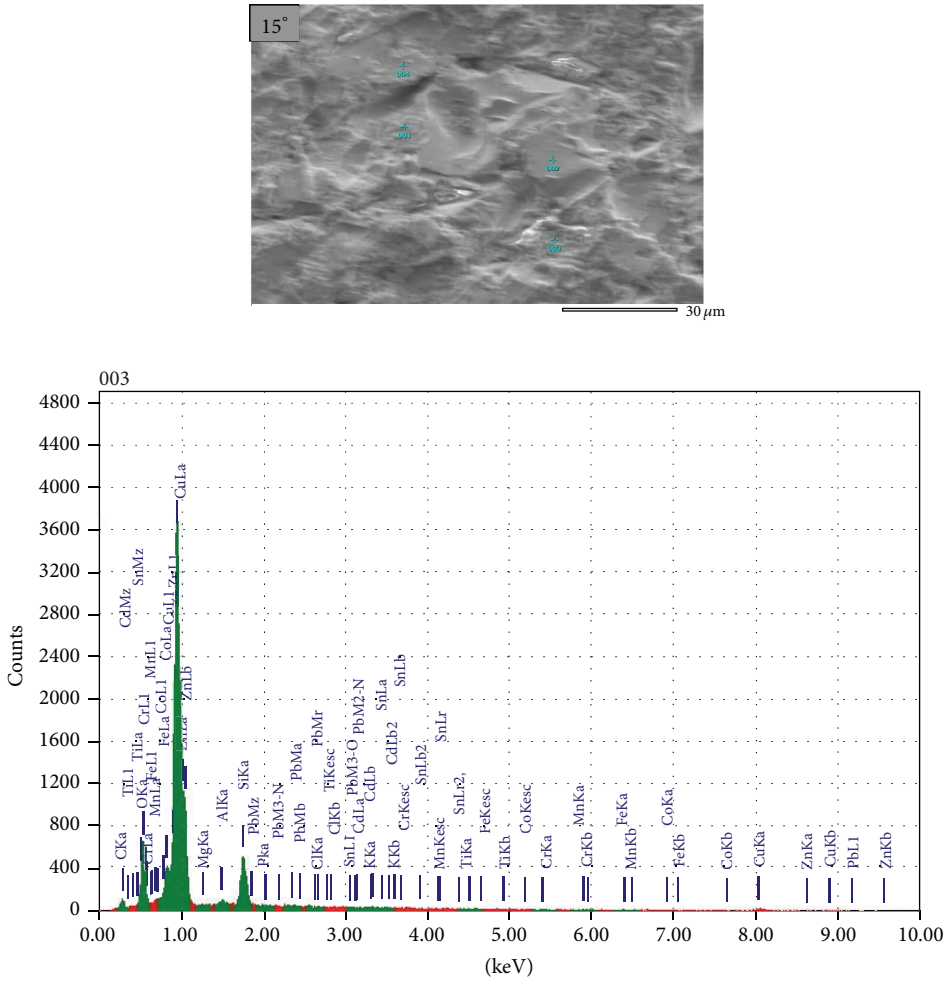

Element		(keV)	Mass (%)	Sigma	Atom (%)
C K		0.277	4.98	0.12	16.01
O K		0.525	11.61	0.17	28.01
Mg K		1.253	0.27	0.06	0.42
Al K		1.486	0.40	0.06	0.57
Si K		1.739	6.42	0.15	8.81
P K		2.013	0.05	0.05	0.06
Cl K					
K K		3.312	0.39	0.09	0.38
Ti K					
Cr K		5.411	0.68	0.19	0.50
Mn K					
Fe K		6.398	0.67	0.25	0.46
Co L	*				
Cu L		0.930	49.41	0.37	30.00
Zn L		1.012	24.89	0.45	14.69
Cd L	*				
Sn L		3.442	0.23	0.19	0.07
Pb M					
Total			100.00		100.00

Figure 22: Energy dispersed X-ray spectrograph (EDX) aluminum alloy at 15-degree impact angle.

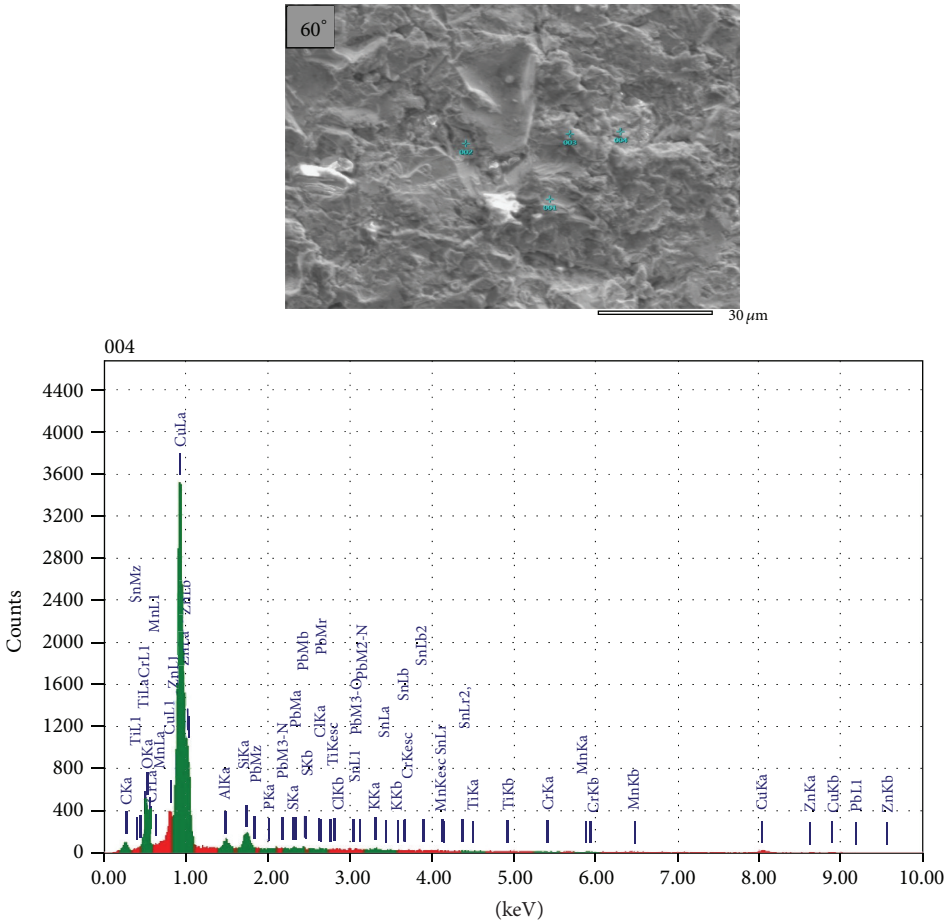

Element		(keV)	Mass (%)	Sigma	Atom (%)
C K		0.277	4.66	0.12	16.34
O K		0.525	9.18	0.16	24.15
Al K	*	1.486	1.21	0.08	1.89
Si K		1.739	2.35	0.11	3.52
P K					
S K		2.307	0.10	0.05	0.14
Cl K					
K K	*	3.312	0.68	0.10	0.74
Ti K	*				
Cr K		5.411	0.15	0.18	0.12
Mn K	*	5.894	0.51	0.23	0.39
Cu L		0.930	51.98	0.40	34.42
Zn L		1.012	27.91	0.50	17.97
Sn L		3.442	0.43	0.21	0.15
Pb M	*	2.342	0.82	0.22	0.17
Total			100.00		100.00

Figure 23: Energy dispersed X-ray spectrograph (EDX) aluminum alloy at 60-degree impact angle.

and stand-off distance. The EDX analysis shows that the percentages of embedded silica are increased with the decrease of percentage of gunmetal for all tested angles. The significance of these observations is that the higher the percentage of copper in gunmetal, the lower the silica engagement within the target surfaces which causes lower erosion rate. Erosion rate is maximum at 15° impingement angle for gunmetal at different impact velocities and particle size. At impact angle 15° erosion rate is high and then decreases gradually up to the impingement angle 45°. After that erosion rate increases ranging from 45° to 90°, in general, for all tested samples. The experimental results also show that erosion rates are slightly higher at 60° impingement angle in most cases as compared to 45°, 75°, and 90° impingement angle.

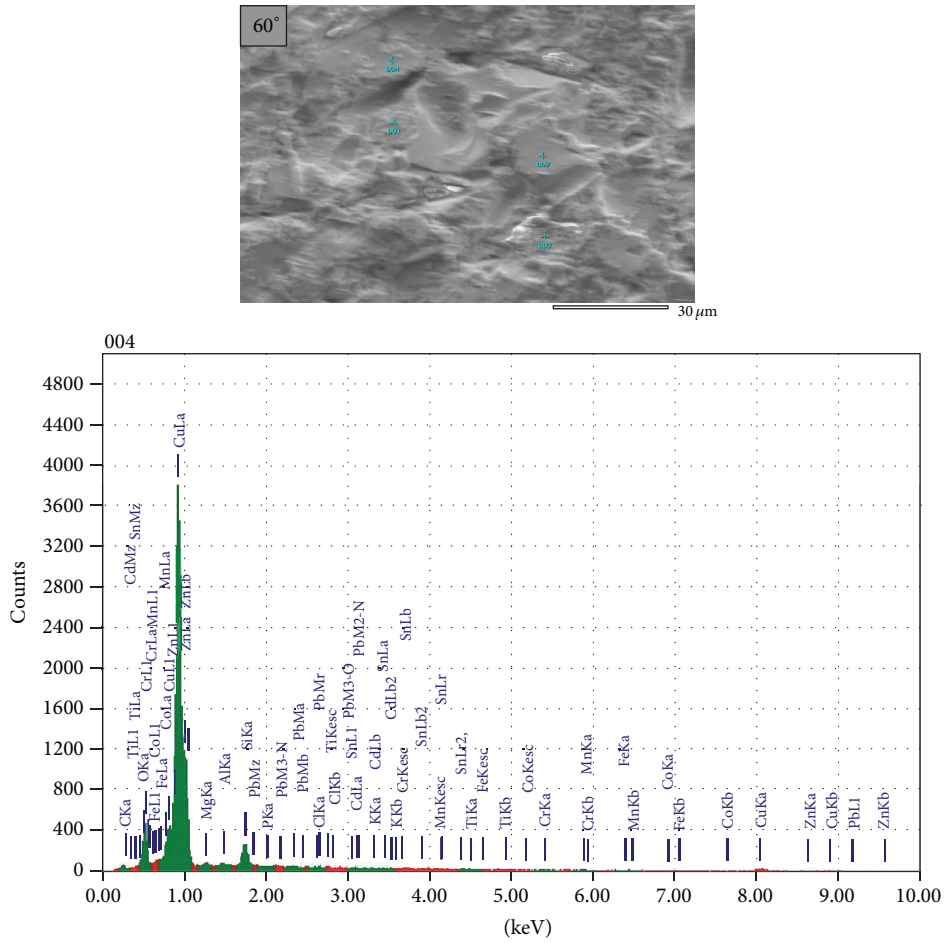

Element		(keV)	Mass (%)	Sigma	Atom (%)
C K		0.277	1.91	0.08	7.43
O K		0.525	7.69	0.14	22.50
Mg K		1.253	0.22	0.06	0.43
Al K		1.486	0.23	0.06	0.40
Si K		1.739	3.43	0.12	5.72
P K		2.013	0.00	0.05	0.01
Cl K		2.621	0.20	0.05	0.26
K K					
Ti K					
Cr K		5.411	0.68	0.19	0.61
Mn K		5.894	1.48	0.26	1.26
Fe K		6.398	0.86	0.27	0.72
Co L	*				
Cu L		0.930	54.52	0.40	40.18
Zn L		1.012	28.43	0.49	20.37
Cd L	*	3.132	0.18	0.15	0.08
Sn L		3.442	0.07	0.18	0.03
Pb M		2.342	0.11	0.20	0.02
Total			100.00		100.00

Figure 24: Energy dispersed X-ray spectrograph (EDX) aluminum alloy at 60-degree impact angle.

The confirmation of ductile category has been ensured by identifying the highest erosion damage at an angle of 15 degrees. The increase of erosion in such fashion with impact velocity and probable kinetic energy level and temperature propagation through the area of tested surface has some exceptional characteristics of the gunmetal. The power law conception based approach ensures the validity of tested gunmetal group by confirming the value of exponent "n"

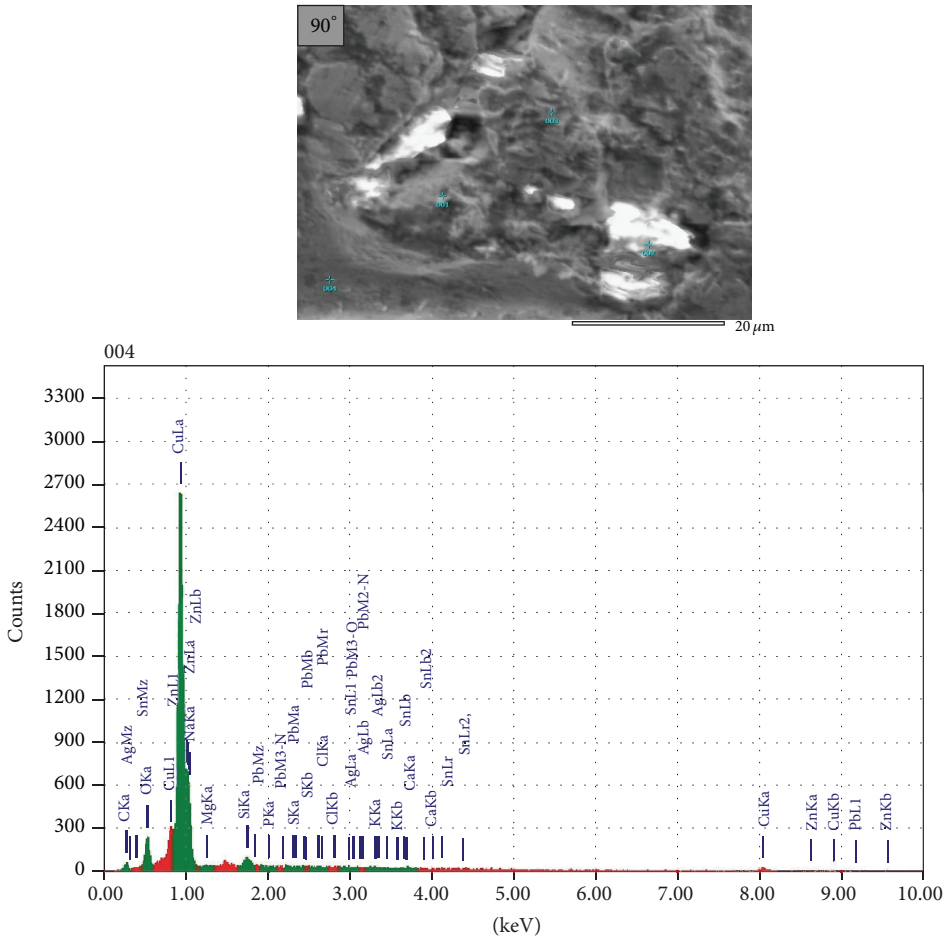

Element		(keV)	Mass (%)	Sigma	Atom (%)
C K	*	0.277	4.09		41219174432768.00
O K		0.525	6.60		84661069938688.00
Na K	*	1.041	3.18		78366518542336.00
Mg K	*	1.253	0.30		24638197334016.00
Si K		1.739	1.50		51467511660544.00
P K					
S K	*				
Cl K	*	2.621	0.11		14744647892992.00
K K	*	3.312	0.27		28667656798208.00
Ca K	*	3.690	0.29		32092805136384.00
Cu L	*	0.930	60.98		289886770823168.00
Zn L	*	1.012	22.44		257352141897728.00
Ag L	*				
Sn L	*	3.442	0.24		36729704677376.00
Pb M	*				
Total			100.00		100.00

Figure 25: Energy dispersed X-ray spectrograph (EDX) aluminum alloy at 90-degree impact angle.

within range 0.7804 to 0.913 and the rage mostly depends on the impact velocity, particular shape of erodent, and particle size rather than impact angle. The correlation of erosion rate with U. No. and relationship between erosion rate and friction factor provide very good agreement. This correlation can be used as a significant tool for future study. The erodent size and stand-off distance provide new insight into relation of these parameters with erosion rate under clarification of possible trends. The average S/N ratio −64.866 dB and Taguchi design concept ensure the validation of experimental and theoretical results. The predicted and experimental S/N ratio fluctuations within range 1.72% and predicted and

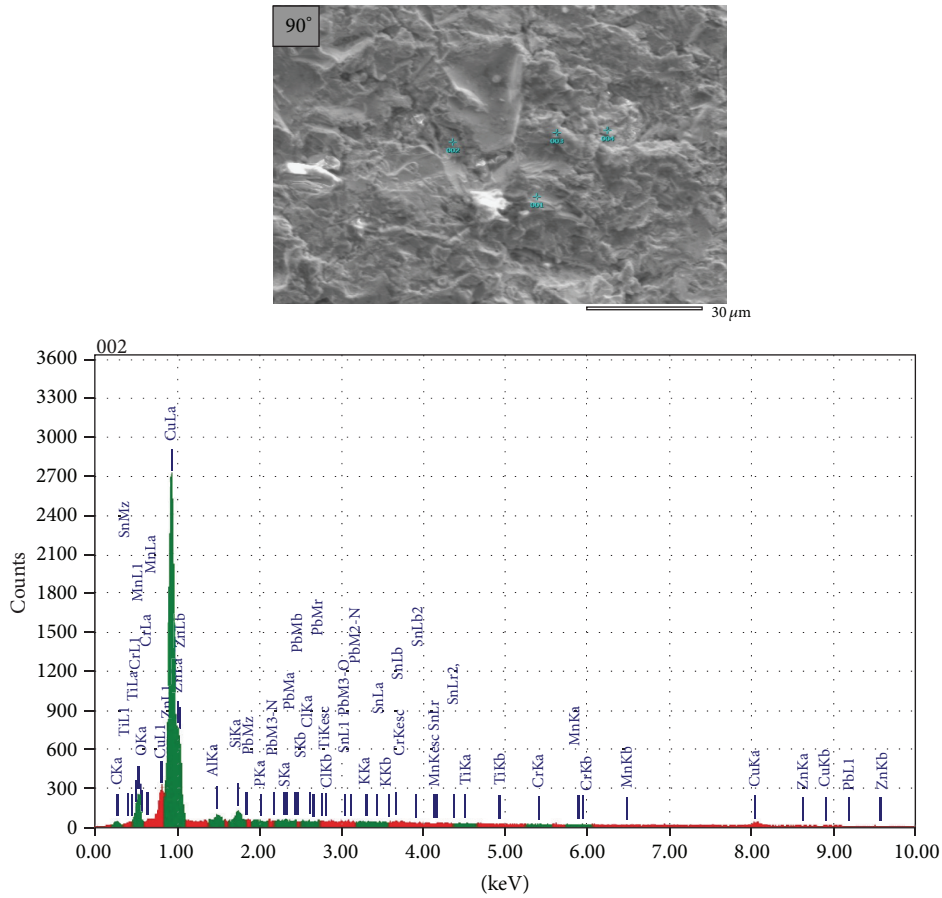

Element		(keV)	Mass (%)	Sigma	Atom (%)	Comp.
C K		0.277	2.24	941996900352.00		9.13
O K		0.525	5.90	2428828909568.00		18.0
Al K	*	1.486	0.90	1251329966080.00		1.63
Si K		1.739	1.86	1759537922048.00		3.23
P K						
S K		2.307	0.15	482571943936.00		0.22
Cl K						
K K	*					
Ti K	*	4.508	0.28	1276800925696.00		0.29
Cr K						
Mn K	*	5.894	0.21	1674659889152.00		0.18
Cu L		0.930	60.25	8727126605824.00		46.3
Zn L		1.012	27.75	8668528508928.00		20.7
Sn L						
Pb M	*	2.342	0.47	1350037143552.00		0.11
Total			100.00		100.00	

Figure 26: Energy dispersed X-ray spectrograph (EDX) aluminum alloy at 90-degree impact angle.

tested model generated by GMDH and 3D explanations are the promising understanding of this newly tested gunmetal. ANOVA method ensures the identity of main dominating factors distinctly or as an interaction on erosion of the tested gunmetal.

It is expected that the analysis of this new or novel concern relating to gunmetal can be used as authentic sources in industry and future researches for the applications of this material in different concerned mechanical and tribological systems.

Conflict of Interests

The authors declare that there is no conflict of interests regarding the publication of this paper.

References

[1] I. Finnie and K. Natesan, "The mechanism of erosion wear in ductile material," in *Corrosion Behaviour of Materials*, pp. 118–126, TMS-AIME, 1980.

[2] S. G. Sapate and A. V. Ramarao, "Erosive wear behaviour of weld hardfacing high chromium cast irons: effect of erodent particles," *Tribology International*, vol. 39, no. 3, pp. 206–212, 2006.

[3] W. Zhu and Z. Y. Mao, "Wear of material," in *Proceeding of Conference Wear of Material*, K. C. Ludema, Ed., p. 787, ASME, 1987.

[4] H. He, J. Nie, and J. Wang, "Impacts of limestone particle size on the performance of flexible wood fiber composite floor," *Advances in Materials Science and Engineering*, vol. 2015, Article ID 804729, 5 pages, 2015.

[5] G. Gupta and A. Satapathy, "Studies on erosion behavior of plasma sprayed coatings of glass microspheres premixed with Al_2O_3 particles," *Advances in Tribology*, vol. 2014, Article ID 763601, 11 pages, 2014.

[6] F. Sabri, J. G. Marchetta, K. M. R. Faysal, A. Brock, and E. Roan, "Effect of aerogel particle concentration on mechanical behavior of impregnated RTV 655 compound material for aerospace applications," *Advances in Materials Science and Engineering*, vol. 2014, Article ID 716356, 10 pages, 2014.

[7] A. P. Harsha and D. K. Bhaskar, "Solid particle erosion behaviour of ferrous and non-ferrous materials and correlation of erosion data with erosion models," *Materials & Design*, vol. 29, no. 9, pp. 1745–1754, 2008.

[8] R. Rattan and J. Bijwe, "Carbon fabric reinforced polyetherimide composites: Influence of weave of fabric and processing parameters on performance properties and erosive wear," *Materials Science and Engineering A*, vol. 420, no. 1-2, pp. 342–350, 2006.

[9] A. E. Miller and D. M. Maijer, "Investigation of erosive-corrosive wear in the low pressure die casting of aluminum A356," *Materials Science and Engineering: A*, vol. 435-436, pp. 100–111, 2006.

[10] E. Avcu, S. Fi'dan, M. Özgür Bora, O. Çoban, İ. Taşkiran, and T. Sinmazçeli'k, "Solid particle erosive wear behavior of glass mat reinforced PPS composites: influence of erodent particle size, pressure, particle impingement angle, and velocity," *Advances in Polymer Technology*, vol. 32, no. 1, pp. E386–E398, 2013.

[11] I. Finnie, "Erosion of surfaces by solid particles," *Wear*, vol. 3, no. 2, pp. 87–103, 1960.

[12] J. Yong-Du and W. Tabakoff, "Numerical simulation of a dilute particle flow over tube banks.-Multiphase flow in wells and pipelines," *FED, ASME*, vol. 144, pp. 125–133, 1992.

[13] J. G. A. Bitter, "A study of erosion phenomena," *Wear*, vol. 6, pp. 69–90, 1963.

[14] G. Grant and W. Tabakoff, "An experimental investigation of the erosion characteristics of 2024 aluminum alloy," Tech. Rep., Department of Aerospace Engineering, University of Cincinnati, 1973.

[15] B. S. McLaury, S. A. Shirazi, J. R. Shadley, and E. F. Rybicki, "Modeling erosion in chokes," in *Proceedings of the Fluids Engineering Division Conference*, vol. 1, pp. 773–781, 1996.

[16] M. Menguturk and E. F. Sverdrup, "Calculated tolerance of a large electric utility gas turbine to erosion damage by coal gas ash particles," ASTM Special Technical Publication 664, ASTM, Philadelphia, Pa, USA, 1979.

[17] C. S. Ramesh, R. Keshavamurthy, B. H. Channabasappa, and S. Pramod, "Influence of heat treatment on slurry erosive wear resistance of Al6061 alloy," *Materials & Design*, vol. 30, no. 9, pp. 3713–3722, 2009.

[18] V. B. Nguyen, Q. B. Nguyen, Z. G. Liu, S. Wan, C. Y. H. Lim, and Y. W. Zhang, "A combined numerical–experimental study on the effect of surface evolution on the water–sand multiphase flow characteristics and the material erosion behavior," *Wear*, vol. 319, no. 1-2, pp. 96–109, 2014.

[19] A. K. Jha, R. Batham, M. Ahmed et al., "Effect of impinging angle and rotating speed on erosion behavior of aluminum," *Transactions of Nonferrous Metals Society of China*, vol. 21, no. 1, pp. 32–38, 2011.

[20] M. S. ElTobgy, E. Ng, and M. A. Elbestawi, "Finite element modeling of erosive wear," *International Journal of Machine Tools & Manufacture*, vol. 45, no. 11, pp. 1337–1346, 2005.

[21] J. G. A. Bitter, "A study of erosion phenomena part I," *Wear*, vol. 6, no. 1, pp. 5–21, 1963.

[22] M. Hashish and A. Suresh, "An improved model of erosion by solid particle impact," in *Proceedings of the 7th International Conference on Erosion by Liquid and Solid Impact*, Paper 66, 1988.

[23] J. R. Mohanty, S. N. Das, H. C. Das, T. K. Mahanta, and S. B. Ghadei, "Solid particle erosion of date palm leaf fiber reinforced polyvinyl alcohol composites," *Advances in Tribology*, vol. 2014, Article ID 293953, 8 pages, 2014.

[24] T. H. Tsiang, "Sand erosion of fiber composites testing and evaluation for design allowable composites ceramics," in *ASTM STP 1003*, pp. 155–174, American Society for Testing and Materials, Philadelphia, Pa, USA, 1989.

[25] R. Balasubramaniam, J. Krishnan, and N. Ramakrishnan, "A study on the shape of the surface generated by abrasive jet machining," *Journal of Materials Processing Technology*, vol. 121, no. 1, pp. 102–106, 2002.

[26] A. G. Evans, M. E. Gulden, and M. Rosenblatt, "Impact damage in brittle materials in the elastic–plastic regime," *Proceedings of the Royal Society of London. Series A*, vol. 361, no. 1706, pp. 343–365, 1978.

[27] A. P. Harsha and D. K. Bhaskar, "Solid particle erosion behaviour of ferrous and non-ferrous materials and correlation of erosion data with erosion models," *Materials and Design*, vol. 29, no. 9, pp. 1745–1754, 2008.

[28] A. Raykowski, M. Hader, B. Maragno, and J. K. Spelt, "Blast cleaning of gas turbine components deposit removal and substrate deformation," *Wear*, vol. 249, no. 1-2, pp. 127–132, 2001.

[29] G. I. Parslow, D. J. Stephenson, J. E. Strutt, and S. Tetlow, "Investigation of solid particle erosion in components of complex geometry," *Wear*, vol. 233–235, pp. 737–745, 1999.

[30] M. Divakar, V. K. Agarwal, S. N. Singh, and J. G. A. Bitter, "A study of erosion phenomena-part I," *Wear*, vol. 6, pp. 15–29, 1988.

[31] J. G. A. Bitter, "A study of erosion phenomena. Part II," *Wear*, vol. 6, no. 3, pp. 169–190, 1963.

[32] B. K. Gandhi and S. V. Borse, "Effects of particle size and size distribution on estimating erosion wear of cast iron in sand-water slurries," *Indian Journal of Engineering and Materials Sciences*, vol. 9, no. 6, pp. 480–486, 2002.

[33] N. Miyazaki and T. Hamao, "Solid particle erosion of thermoplastic resins reinforced by short fibers," *Journal of Composite Materials*, vol. 28, no. 9, pp. 871–883, 1994.

[34] H. M. Clark and L. C. Burmeister, "Influence of the squeeze film on particle impact velocities in erosion," *International Journal of Impact Engineering*, vol. 12, no. 3, pp. 415–426, 1992.

[35] M. M. Stack and N. Pungwiwat, "Slurry erosion of metallics, polymers, and ceramics: particle size effects," *Materials Science and Technology*, vol. 15, no. 3, pp. 337–344, 1999.

[36] G. R. Desale, B. K. Gandhi, and S. C. Jain, "Effect of physical properties of solid particle on erosion wear of ductile materials," in *Proceedings of the 3rd ASME World Ribology Congress*, Washington, DC, USA, Sepetember 2005.

[37] G. Sundararajan and M. Roy, "Solid particle erosion behaviour of metallic materials at room and elevated temperatures," *Tribology International*, vol. 30, no. 5, pp. 339–359, 1997.

[38] D. P. Mondal, S. Das, A. K. Jha, and A. H. Yegneswaran, "Abrasive wear of Al alloy-Al_2O_3 particle composite: a study on the combined effect of load and size of abrasive," *Wear*, vol. 223, no. 1-2, pp. 131–138, 1998.

[39] M. Dundar and O. T. Inal, "Solid particle erosion of α-brass with 5 and 25 μm particles at normal incidence," *Wear*, vol. 224, no. 2, pp. 226–235, 1999.

[40] R. S. Lynn, K. K. Wong, and H. M. Clark, "On the particle size effect in slurry erosion," *Wear*, vol. 149, no. 1-2, pp. 55–71, 1991.

[41] H. M. Clark and R. B. Hartwich, "A re-examination of the 'particle size effect' in slurry erosion," *Wear*, vol. 248, no. 1-2, pp. 147–161, 2001.

[42] G. Stachowiak and A. W. Batchelor, *Engineering Tribology*, Butterworth, 2nd edition, 2005.

[43] G. Sundararajan, M. Roy, and B. Venkataraman, "Erosion efficiency—a new parameter to characterize the dominant erosion micromechanism," *Wear*, vol. 140, no. 2, pp. 369–381, 1990.

[44] S. Arjula, A. P. Harsha, and M. K. Ghosh, "Erosive wear of unidirectional high carbon steel materials," *Materials Letters*, vol. 62, pp. 3246–3249, 2006.

[45] A. Mishra, M. Martin, N. N. Thadhani, B. K. Kad, E. A. Kenik, and M. A. Meyers, "High-strain-rate response of ultra-fine-grained copper," *Acta Materialia*, vol. 56, no. 12, pp. 2770–2783, 2008.